Theory of Transport Processes in Single Crystal Growth from the Melt

The quality of large semiconductor crystals grown from the melt for use in electronic and optoelectronic devices is strongly influenced by the intricate coupling of heat and mass transfer and melt flow in growth systems. This paper reviews the present state of understanding of these processes starting from the simplest descriptions of solidification processes to detailed numerical calculations needed for quantitative modeling of processing with solidification. Descriptions of models for the vertical Bridgman-Stockbarger and Czochralski crystal growth techniques are included as examples of the level of understanding of industrially important methods.

Robert A. Brown
Department of Chemical Engineering and
Materials Processing Center
Massachusetts Institute of Technology
Cambridge, MA 02139

Introduction

Melt crystal growth of semiconductor materials is a mainstay of the microelectronics industry. Boules of nearly perfect crystals are grown by a variety of techniques for controlled solidification and are used as substrates in almost all device fabrication technologies. The variety of crystalline materials produced in this manner ranges from the ubiquitous silicon to more exotic materials such as GaAs, InP, and CdTe. Although the processing conditions for each of these materials differ in some details, the solidification systems are similar in that the system dynamics and the quality of the crystal produced are governed by the same set of concepts describing the transport processes, thermodynamics, and materials science. These underpinnings make melt crystal growth one of the "unit operations" of electronic materials processing and motivate the presentation in this paper.

Many review papers and several books (Flemings, 1974; Brice, 1976; Rosenberger, 1979) have focused on the science and technology of crystal growth. The purpose of this review is not to duplicate these works, but to focus on the fundamental transport processes that occur in melt crystal growth systems, especially advances in understanding that have occurred in the last decade of vigorous research. The paper also accentuates the features and research issues that are common to many of the techniques used today in laboratories and industrial production.

A thorough understanding of heat and mass transport in melt growth processes is a prerequisite to optimization of these systems for control of crystal quality, as measured by the degree of crystallographic perfection of the lattice and the spatial uniformity of electrically active solutes in it. The discussion here focuses on the role of transport processes in controlling the stability of melt growth techniques and in setting the solute segregation in the crystal. Several review papers have also discussed these aspects (Pimputkar and Ostrach, 1981; Brown, 1987b).

The connection between processing conditions and crystalline perfection is incomplete because the link is missing between microscopic variations in the structure of the crystal and macroscopic processing variables. For example, studies that attempt to link the temperature field with dislocation generation in the crystal assume that defects are created when the stresses due to linear thermoelastic expansion exceed the critically resolved shear stress for a perfect crystal. The status of these analyses and the unanswered questions that must be resolved for precise coupling of processing and crystal properties are described in a later subsection on the connection between transport processes and defect formation in the crystal.

The simple models of transport processes in controlled solidification, solute redistribution, and process stability reviewed here are based on results of pioneering studies in the last three decades. The analyses are rich in physical insight, but are semiquantitative because of the limiting assumptions needed to permit closed-form analysis. The new possibilities for large-scale numerical analysis of these transport processes are beginning to make practical the detailed simulation of melt growth. Examples of these results are included to give perspective on the complexity involved in quantitative modeling of these systems.

Several examples of melt growth systems are described in the next section to facilitate the description of the transport processes in the succeeding section. The crystal growth systems are distinguished according to whether a surrounding solid ampoule

or a melt/fluid meniscus shapes the crystal near the solidification interface. Methods with these features are classified as confined and meniscus-defined crystal growth techniques, respectively. Following that, the fundamental transport processes associated with solidification of a dilute binary alloy in a temperature gradient are reviewed. The classical one-dimensional analysis of directional solidification is discussed for diffusion-controlled growth. Then mechanisms for convection in the melt are reviewed and models for accounting for convection in solute transport are presented.

Progress in analysis and optimization of real solidification systems is exemplified in later sections through descriptions of the vertical Bridgman-Stockbarger and Czochralski growth methods. The meniscus-defined growth of the Czochralski method leads to the issues of process stability and control for batchwise growth; these points are brought out in a subsection devoted to process stability and control.

Table 1. Common Semiconductor Materials and Methods Used to Grow Them from the Melt

Material	Application	Technique
Single-crystal silicon	Integrated circuits	Czochralski
High-resistivity single-crystal silicon	Power transistors	Floating zone
Polycrystalline silicon	Photovoltaic devices	Variety of meniscus-defined growth techniques
III-V materials e.g., GaAs, InP	Optoelectronic devices; integrated circuits	Horizontal boat; horizontal Bridgman; liquid-encapsulated Czochralski; vertical gradient freeze
II-VI materials e.g., CdTe, HgCdTe	Detectors	Vertical Bridgman; horizontal Bridgman

Classification of Melt Crystal Growth Systems

Important development efforts have gone into any crystal growth method that is being used for the growth of production materials to attempt to optimize the important aspects of each process with respect to the production of compositionally uniform cylindrical crystals with low densities of crystallline defects. The many technological innovations in melt crystal growth of semiconductor materials all build on the two basic concepts of confined and meniscus-defined crystal growth. Examples of these two systems are shown schematically in Figure 1. Typical semiconductor materials grown by these and other methods are listed in Table 1. The discussion in this section focuses on some of the design variables for each of these methods that affect the quality of the product crystal. The remainder of the paper addresses the relationship between these issues and understanding transport processes in crystal growth systems.

Several issues must be addressed. First, the heat transfer environment must yield a well-controlled temperature field in the crystal and melt near the melt/crystal interface so that the crystallization rate, the shape of the solidification interface, and thermoelastic stresses in the crystal can be controlled. As is brought out later, low dislocation and defect densities occur when the temperature gradients in the crystal are low. This point will become an underlying theme of this paper and has manifestations in analysis of many of the transport processes described here.

Second, the stoichiometry of the melt and of impurities introduced during processing must be controlled to the level demanded by application. Although these constraints vary with application, it is clear that more control is better in that the demands on purity and spatial uniformity of the material are becoming more stringent with increasing miniaturization of electronic devices.

Confined crystal growth systems

In confined growth geometries, such as the variations of the directional solidification method (Flemings, 1974), the material

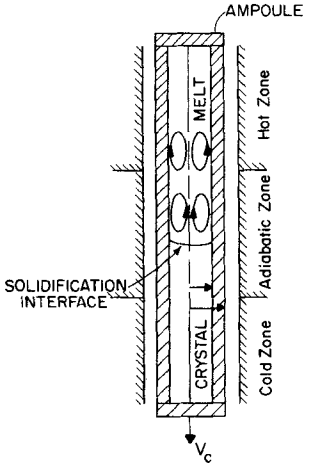

Figure 1a. Vertical Bridgman-Stockbarger method

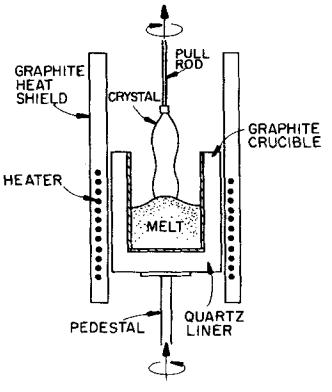

Figure 1b. Czochralski method

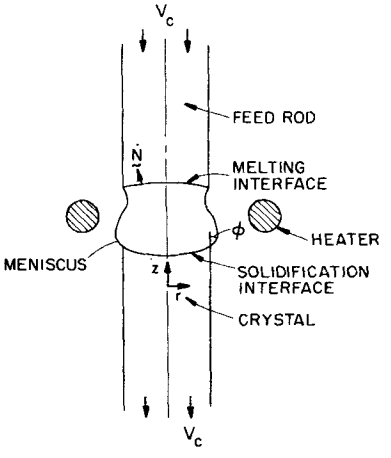

Figure 1c. Small-scale floating zone method

Figure 1. Commonly used systems for melt crystal growth of electronic materials.

is loaded into an ampoule, melted, and resolidified by varying the temperature field either by translating the ampoule through the furnace (the Bridgman-Stockbarger method, Figure 1a) or by time-dependent variation of the heater power (the gradient freeze method). After solidification, the material is removed from the ampoule.

Confined melt growth systems have been used primarily for laboratory preparation of exotic materials and for alloys with high vapor pressures, where control of the stoichiometry in the melt is difficult without confinement; see Table 1. Directional solidification and the gradient freeze techniques are becoming popular for the growth of GaAs, InP, and other materials where low axial temperature gradients are needed to produce crystals with low dislocation densities. Some of the renewed interest in these methods is a result of improvements in the control of the temperature gradients. Carefully designed heat-pipe furnaces have been successfully used in Bridgman-Stockbarger systems (Wang, 1984), but have been limited to temperatures below 1,100°C. Multizone resistance furnaces have found application in gradient freeze systems operating at higher temperatures (Parsey and Thiel, 1985; Gault et al., 1986) for the growth of InP, GaP, and GaAs.

The horizontal Bridgman or boat growth technique, is a variant in which the ampoule is laid horizontally with respect to gravity and the temperature gradient in the melt is changed by varying the temperature profile in the surrounding heater. The melt is contained in an open ampoule, or boat, so that the composition of the melt can be equilibrated with the surrounding ambient. For GaAs growth, a source of arsenic is placed in the system and the vapor pressure of arsenic is controlled independently to maintain the stoichiometry of the melt. This technique is a hybrid of the classical gradient freezing technique, because of the method for varying the temperature profile, and of a meniscus-defined growth method, because of the presence of the melt/ambient surface.

Meniscus-defined crystal growth systems

In most conventional meniscus-defined growth systems a seed crystal is dipped into a pool of melt and the thermal environment is varied so that a crystal grows from the seed as it is pulled slowly out of the pool. Two examples of meniscus-defined growth are shown in Figure 1. The Czochralski method (CZ) shown there, Figure 1b, and the closely related liquid-encapsulated Czochralski (LEC) method are batchwise processes where the crystal is pulled from a crucible with decreasing melt volume. In the LEC system an oxide material (usually B_2O_3) is layered over the melt to prevent the loss of volatile components in a high vapor pressure system such as GaAs and InP. The gas pressure is usually maintained significantly above ambient in these systems.

Reviews have been published describing the details for implementation of Czochralski crystal growth (Zulehner and Huber, 1982; Hurle, 1985; Lin and Benson, 1987), the floating zone method (Pfann, 1978; Muhlbauer and Keller, 1981), and meniscus-defined growth methods developed for producing thin sheets (Ciszek, 1984; Dietl et al., 1981). The advantages and disadvantages of various confined and meniscus-defined growth methods determine the types of materials that are produced by each technique. For example, meniscus-defined methods have the advantage that the cooling crystal is free to expand and so is less likely to generate large thermoelastic stresses that lead to defect and dislocation generation. However, active control is needed to produce crystals of uniform cross section because the shape of the crystal is constrained only by capillary action.

In the floating zone (FZ) system a molten pool is formed by a circumferential heat source that separates a melting polycrystalline feed rod and a solidifying cylindrical crystal. In small-scale, resistively heated zones, the pool of melt is held in shape by capillary forces and gravity and by hydrodynamic stresses caused by flow in the melt. The experimental techniques related to floating zone systems are discussed in the pioneering book by Pfann (1978). Floating zone systems with conventional resistance heaters are limited on earth to the growth of crystals with diameters less than approximately 1 cm because deformation of the meniscus by gravity causes loss of wetting of the crystal by the surrounding melt (Duranceau and Brown, 1986); floating zone growth in outer space removes this restriction and is an active area of research (Brown, 1986). The shape of a small-scale floating zone is shown in Figure 1c.

Large-diameter industrial floating zone systems have been developed using radio-frequency (RF) induction heating elements shaped so that the induction coil has a smaller diameter than the growing crystal. These systems are used for growth of high-purity semiconductor materials, such as high-resistivity silicon and germanium, and are described in the book by Muhlbauer and Keller (1981). The explanation for the success of these systems has centered on the levitation of the melt caused by the Maxwell stresses induced by the coil; however; appeal to meniscus stabilization because of this additional levitation force may not be necessary considering the shape of the zone. The large melting interface of the polycrystalline feed rod is typically very concave so that the distance between the two melt/solid interfaces is small, perhaps no more than a centimeter. The melting interface is covered with a thin film of melt so that the meniscus surrounding bulk fluid exists only adjacent to the crystal and the molten zone may be no larger in the system with RF heating than when resistive heating is used for smaller diameter crystals. From this point of view the RF coil is a cleaver method of locally heating a small melt pool that is bound by a meniscus with a shape that balances capillary force with gravity.

Issues in modeling melt crystal growth systems

Two key issues must be addressed before a detailed survey of the modeling of melt crystal growth is presented. First, it must be clear why, and on what levels, modeling can play a role in the optimization and control of systems for the growth of single crystals from the melt. All that is needed to see the potential for modeling in the development of these processes is a survey of the current state of the art in the growth of different semiconductor materials by similar processes.

Variants of the CZ process make a good case study. In the last quater-century, the Czochralski process has been optimized for the growth of single-crystal silicon to the point that today dislocation-free crystals with 4–6 in. (10–15 cm) diameters are grown from 5–25 kg batches of melt. The diameter control is 0.1% and impurity levels are controlled to be less than 5×10^{15} carbon and 1×10^{18} oxygen atoms/cm^3. By contrast, GaAs crystals grown by the liquid-encapsulated Czochralski process are limited to less than 3 in. (7.6 cm) dia. with poor diameter con-

trol, and have between 300–5,000 dislocations/cm^2, depending on the level of dopants added to the melt. Moreover, other semiconductor materials, such as CdTe, have not been grown successfully in Czochralski configurations. The difference in difficulty for producing silicon and GaAs wafers is reflected in the factor of 100 difference in their cost per square centimeter.

The role of transport processes in setting the level of difficulty for growth of each of these materials was described qualitatively by S. Motakeff at M.I.T. in terms of a plot similar to Figure 2 where the estimated thermal conductivities of several semiconductor materials are plotted against the appropriate values of the critical resolved shear stress (CRSS). Materials with low conductivities and low values of CRSS are more difficult to grow because of the large temperature gradients (proportional to the conductivity) that will occur during processing and the lower resistance of the crystal to the formation of dislocations (proportional to CRSS). Although this argument is extremely qualitative, the trend is clear. Analysis of linear thermoelastic stress will be developed further in a later subsection on transport processes and defect formation. The newer materials used in the microelectronics industry can be produced only with better quantitative optimization and control of the growth systems. Modeling will play a substantial role in the development of the next generation of crystal growth systems.

Analysis of crystal growth systems transcends levels of detail ranging from thermal analysis of an entire crystal growth system to analysis of the dynamics of defects in the crystal lattice. These models are represented schematically in Figure 3 for a vertical Bridgman growth system. Several intermediate-length scales for modeling this system have been included that are not obvious without further discussion of the transport processes. These are an intermediate scale for analysis of melt flow and solute transport in the melt with boundary conditions imposed by coupling between this level of detail and an entire system model, and microscale models of melt/crystal interface morphology that account for surface forces and crystalline anisotropy. Analyses on these three length scales are based on continuum conservation equations and are described in this paper.

Defect formation and dynamics in the crystal and at the melt/crystal interface are molecular -scale events that are only adequately stimulated by lattice-scale models. A thorough discussion of lattice-scale equilibrium and molecular dynamics calculations is beyond the scope of this paper.

An important question for any modeling effort, especially one aimed at a quantitative description of complex transport processes, is the level of accuracy of the model. As will become evident in the discussion of transport models and specific calculations, it is crucial to know the values for thermophysical properties and transport coefficients, as well as the dependence of these coefficients on temperature and pressure. There is a dearth of information for this database. Critical material properties for semiconductor materials are not known with any accuracy, let alone are any data available on the sensitivity of the parameters to temperature and concentration. For example, the value of the coefficient of thermal expansion for molten silicon is only available from two isolated measurements, which disagree by a factor of three (Langlois, 1982). The difference is this number is critical in predicting whether steady or time-dependent flow occurs in simulations of buoyancy-driven convection in CZ crystal growth. Thermophysical properties for important III-V semiconductors are almost totally unknown; Jordan (1985) has compiled the available data and has estimated properties for GaAs and InP. The value of such estimates is now being questioned. For example, recent measurements of the viscosity of molten GaAs over a range of temperatures show an order-of-magnitude increase as the melting point is approached (Kakimoto and Hibiya, 1987). The authors suggest that molecular association in the melt is responsible for the increase.

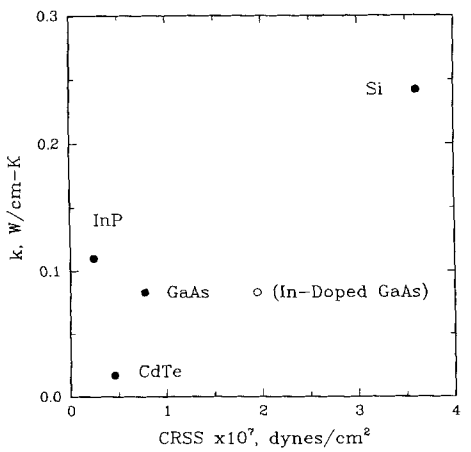

Figure 2. Thermal conductivity of common semiconductor materials vs. best estimates for critical resolved shear stress (CRSS).

Materials with low thermal conductivity and low CRSS are hardest to grow

Basic Transport Processes in Directional Solidification

The simplest picture of a directional solidification process is shown schematically in Figure 4 and corresponds to melt translating through a temperature field established by a surrounding furnace that brackets the melting temperature. When convective heat transport is unimportant, the temperature in the melt and crystal is idealized as a nearly constant axial gradient for the purpose of describing the basic transport mechanisms. The quantitative details of the temperature field depend on the thermophysical properties of the melt, the crystal, and the surrounding ampoule and on the growth rate through latent heat release at the solidification interface. In a confined growth system, convection in the melt is caused by the translation of the ampoule and by buoyancy-driven convection due to temperature and concentration gradients. The details of the convection pattern will depend on heat transfer in the system and on the orientation of the melt and crystal with respect to gravity.

Heat transfer in melt crystal growth systems is by conduction in all phases, by convection in the melt, and by convective, conductive, and radiation exchange between the various parts of the growth system. The goal of the design of heat transfer systems for any crystal growth configuration is to establish a nearly constant temperature gradient laterally along the melt/crystal interface and to control the cooling rate of the crystal. The details of implementing these conditions can be extremely complex because of the complicated geometries in systems like the CZ and LEC techniques and because of the influence of radiative heat exchange. Progress in understanding heat transport is discussed for specific systems in the later sections on vertical Bridgman-Stockbarger and Czochralski crystal growth. The

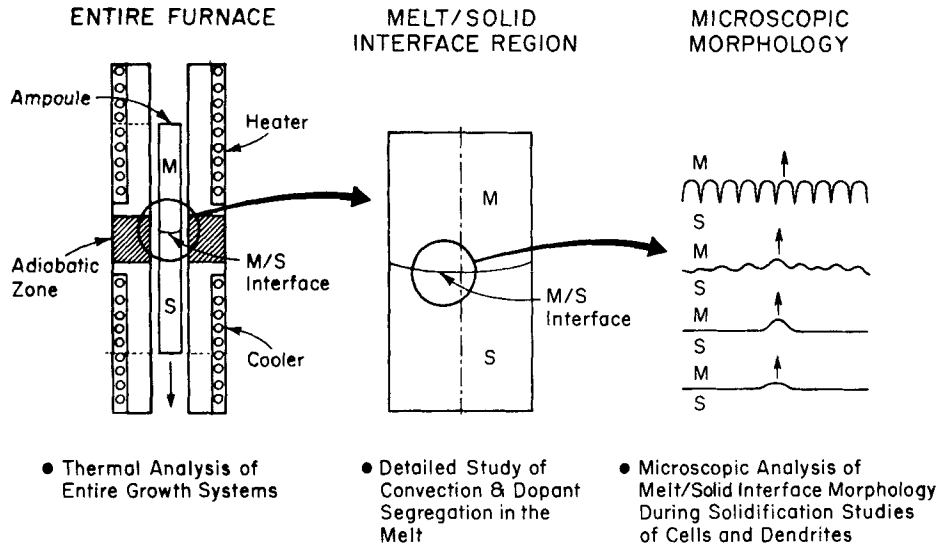

Figure 3. Three spatial scales for modeling melt crystal growth, as exemplified by the vertical Bridgman system.

discussion here focuses on species transport for solutes that form ideal solutions in the melt and single-phase crystalline solids. The shape of the phase diagram between melt and solid is described by the dependence of the liquidus $T_s(c)$ and solidus $T_l(s)$ temperatures on the solute concentration c. The liquidus and solidus curves are taken to be straight lines with slopes m and m/k, respectively, where k is the equilibrium partition coefficient. Then the composition of melt and solid in equilibrium are related by

$$\tilde{c}_m = \tilde{c}_s/k \tag{1}$$

(The symbol (˜) is used throughout this paper to denote dimensional variables; the absence of it corresponds to a dimensionless formulation.) The phase diagram corresponding to constant values of m and k is shown in Figure 5.

Taking the segregation coefficient to be independent of the local growth rate of the crystal is to assume that the solute concentration is in local equilibrium at the interface, i.e., that interface kinetics play no role in setting the composition of the crystal. Although this assumption is probably accurate for the slow growth rates (1–10 μm/s) on a microscopically rough crystal surface typical for the growth of many semiconductors, it is undoubtedly poor at higher solidification velocities or when the crystal grows along a facet so that the growth rate is governed by the movement of ledges across the surface.

One-dimensional, diffusion-controlled crystal growth

Neglecting bulk convection leads to an idealized picture of diffusion-controlled solute transport of a dilute binary alloy with the solute composition c_0 far from an almost flat melt/crystal interface located at $\tilde{z} = 0$ (Tiller et al., 1953; Flemings, 1974). When viewed from a reference frame stationary with the solidification interface, the melt moves uniaxially toward the interface and the crystal moves away. Then solute transport in the melt is governed by the one-dimensional balance equation

$$D\frac{\partial^2 \tilde{c}}{\partial \tilde{z}^2} + V_g \frac{\partial \tilde{c}}{\partial \tilde{z}} = 0 \tag{2}$$

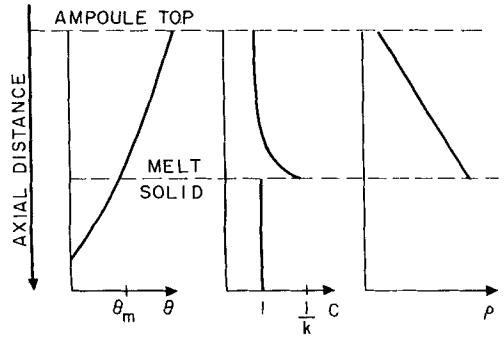

Figure 4. Temperature, solute concentration, and density profiles in one-dimensional directional solidification of a binary alloy.
Profile shapes are justified for analysis described in text for one-dimensional, diffusion-controlled crystal growth

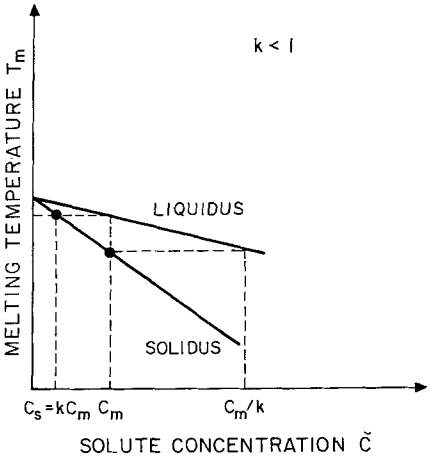

Figure 5. Idealized phase diagram for a binary alloy.
Liquidus slope m and equilibrium segregation coefficient k are defined

where D is the solute diffusivity in the melt and V_g is the growth rate measured in terms of the melt velocity. Equation 2 is solved with the condition of solute conservation at the melt/crystal interface

$$-D\left.\frac{\partial \tilde{c}}{\partial \tilde{z}}\right|_{\tilde{z}=0} = (1-k)\tilde{c}|_{\tilde{z}=0} \tag{3}$$

where k is the equilibrium partition coefficient defined by Eq. 1. Because the growth rate V_g is taken to be independent of the composition at the interface, the results are limited in practice to dilute alloy systems. The solute field that decays to c_0 far ($\tilde{z} \to \infty$) from the interface is

$$\tilde{c}(\tilde{z}) = c_0\left[1 + \frac{1-k}{k}\exp\left(-V_g\tilde{z}/D\right)\right] \tag{4}$$

Equation 4 shows the existence of an exponential diffusion layer adjacent to the interface so that the variation in concentration caused by solute rejection ($k < 1$) or incorporation ($k > 1$) at the interface only persists for an e-folding distance on the order of D/V_g.

Analysis of transients in directional solidification is complicated by the coupling between heat transfer, the melt/crystal interface shape, and solute transport. Smith et al. (1955) analyzed the idealized situation of one-dimensional, diffusion-controlled transport in which the diffusion of heat is much more rapid then that of solute, so that changes in the heat transfer environment or the ampoule pull rate appear as a step change in the macroscopic solidification rate at the interface. Under these conditions the transient solute profile is governed by Eqs. 2 and 3 with an accumulation term ($\partial\tilde{c}/\partial t$) appearing on the right-hand side of Eq. 2. Separation-of-variables solution of this equation and the boundary condition, Eq. 4, gives an e-folding time D/kV_g^2 for the solute profile in response to a step change in the pull rate.

When the alloy is nondilute the melting temperature depends on the solute concentration adjacent to the interface through the shape of the liquidus curve. Then the transport of heat and solute and the location of the solidification interface do not decouple; Bourret et al. (1985), and Derby and Brown (1986a) presented a numerical algorithm for analysis of this problem.

Overview of convection in melt growth

Convection in the melt is pervasive in all terrestrial melt growth systems. Sources for flows include buoyancy-driven convection caused by solute and temperature dependence of the density, surface-tension gradients along melt/fluid menisci, forced convection introduced by the motion of solid surfaces, such as crucible and crystal rotation in the CZ and FZ systems, and the motion of the melt induced by the solidification of material. These flows are important as sources for convection of heat and species, and can have a dominant influence on the temperature field in the system and on solute incorporation into the crystal. Moreover, flow transitions from steady laminar, to time-periodic, chaotic, and turbulent motion cause temporal nonuniformities at the growth interface. These fluctuations in temperature and concentration fluctuations can cause the melt/crystal interface to melt and resolidify and lead to the solute striations (Carruthers and Witt, 1975) discussed below in the subsection on the importance of flow transitions, and the formation of microdefects described later.

The equations of motion and boundary conditions appropriate for describing convection and heat transport in the melt are presented next, as background for the discussion of modeling of these flows. Then progress in asymptotic analysis of simple flows is described.

Equations of Motion and Driving Forces for Convection. The presentation here is limited to the case when the density variations in the melt caused by temperature and concentration gradients can be modeled by the Boussinesq approximation (Turner, 1973) in terms of the thermal and solutal expansion coefficients $\beta_t \equiv (1/\tilde{\rho})\,(\partial\tilde{\rho}/\partial\tilde{T})_{\tilde{p},\tilde{c}}$ and $\beta_c \equiv (1/\tilde{\rho})\,(\partial\tilde{\rho}/\partial\tilde{c})_{\tilde{p},\tilde{T}}$ where p is the pressure. Positive values of β_t correspond to a material with a density that decreases with increasing temperature; a positive value of β_c is appropriate for a solute with density that increases with increasing concentration.

The governing equations and boundary conditions for modeling melt crystal growth are described for the CZ growth geometry shown in Figure 6. The equations of motion, continuity, and transport of heat and of a dilute solute are:

$$\rho_0(\partial\tilde{v}/\partial\tilde{t} + \tilde{v}\cdot\nabla\tilde{v}) = -\nabla\tilde{p} + \mu\nabla^2\tilde{v} + \rho_0 g[1 - \beta_t(\tilde{T} - \tilde{T}_r) + \beta_c(\tilde{c} - c_0)]e_z + \tilde{F}_b(\tilde{v},\tilde{x}) \tag{5}$$

$$\nabla\cdot\tilde{v} = 0 \tag{6}$$

$$[\partial\tilde{T}/\partial\tilde{t} + \tilde{v}\cdot\nabla\tilde{T}] = \alpha_m\nabla^2\tilde{T} \tag{7}$$

$$[\partial\tilde{c}/\partial\tilde{t} + \tilde{v}\cdot\nabla\tilde{c}] = D\nabla^2\tilde{c} \tag{8}$$

where ∇ is the gradient operator, $\tilde{v}(\tilde{x},\tilde{t})$ is the velocity vector field, $\tilde{p}(\tilde{x},\tilde{t})$ is the pressure field, μ is the fluid viscosity, α_m is the thermal diffusivity, and D is the solute diffusivity in the

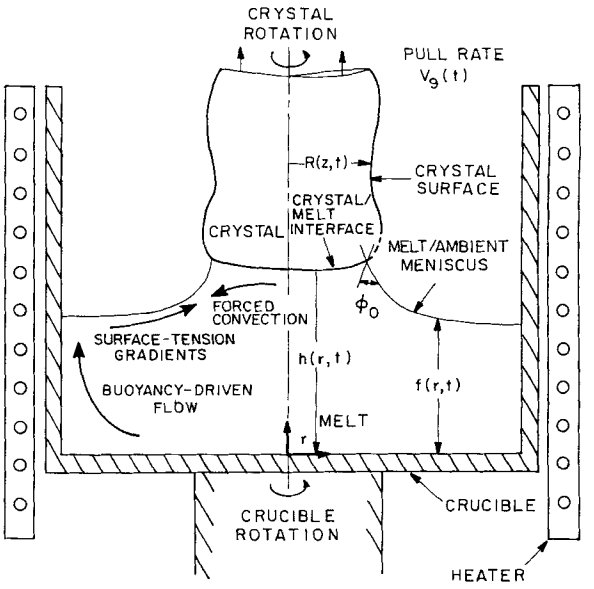

Figure 6. Driving forces for flows in CZ crystal growth system and regions where driving forces will produce the strongest motions.

Shape functions describing the unknown interface shapes are also listed

melt. These and other thermophysical properties are defined in the Notation. The vector $\tilde{F}_b$ is a body force, in addition to gravity, imposed on the melt. The body force caused by an imposed magnetic field $\tilde{B}(\tilde{x}, \tilde{t})$ is the Lorentz force $\tilde{F}_b \equiv \sigma_c(\tilde{v} \times \tilde{v} \times \tilde{B})$. The effect of this field on convection and segregation is discussed below.

Other mechanisms for flows in melt crystal growth arise from surface stresses along, or relative motion of, boundaries of the melt. The no-slip boundary condition describes relative motion of a rigid boundary ∂D_{b1}:

$$\tilde{v}(\tilde{x}, t) = \tilde{V}_s(\tilde{x}, t) \quad \text{for} \quad \tilde{x} \in \partial D_{b1} \tag{9}$$

where $\tilde{V}_s(\tilde{x}, \tilde{t})$ is the velocity of the portion of the boundary ∂D_{b1}. Melt is solidified normal to the melt/solid interface obeys no-slip tangential to the surface. These conditions are written as

$$(N \cdot \tilde{v}) = \tilde{V}_m(N \cdot e_g), (T \cdot \tilde{v}) = \tilde{V}_m(T \cdot e_g), \quad \tilde{x} \in \partial D_{bI} \tag{10}$$

for a steadily solidifying solid, where the shape of the melt/crystal surface is given by the unit normal N and tangent T vectors and the direction of steady-state solidification at the velocity $\tilde{V}_m$ is given by the unit vector e_g.

Both the normal and tangential components of stress must balance and the kinematics of the surface and flow field must be consistent along a melt/fluid interface. For the meniscus shown in Figure 6 and described by the normal and tangent vectors (n, t), these conditions dictate that

$$nn:[-\tilde{p}I + \mu(\nabla\tilde{v} + \nabla\tilde{v}^T)] + p_0 = 2\sigma\tilde{H} + n \cdot \tilde{F}_s \tag{11a}$$

$$[\mu tn:(\nabla\tilde{v} + \nabla\tilde{v}^T)] = \nabla_2\tilde{\sigma} + t \cdot \tilde{F}_s \tag{11b}$$

$$\partial\tilde{h}/\partial\tilde{t} = n \cdot \tilde{v}, \tilde{x} \in \partial D_{bm} \tag{12}$$

where $\tilde{H}$ is the mean curvature of the surface, σ is the interfacial tension, ∇_2 is the gradient operator defined for the surface, and I is the identity tensor. The brackets $[\cdot]$ signify the difference of the quantity evaluated from both phases bordering the meniscus. Equation 11a is the condition for balancing normal stress across the meniscus with the presence of the gas phase accounted for simply by a static pressure p_0. When viscous stresses (the term proportional to the viscosity μ) and the dynamic pressure in the melt are unimportant this condition gives the Young-Laplace equation for the shape of a hydrostatic interface. Solutions for the Young-Laplace equation are available for most meniscus-defined growth configurations.

The term $\nabla_2\sigma$ in Eq. 11b represents the tangential stress caused by a spatial variation in the interfacial tension due to either concentration or temperature variation along the surface. The dependence of the interfacial tension on temperature and concentration is usually expressed by the approximation.

$$\tilde{\sigma} = \sigma_0[1 + (\partial\tilde{\sigma}/\partial\tilde{T})_c(\tilde{T} - T_0) + (\partial\tilde{\sigma}/\partial\tilde{c})_T(\tilde{c} - c_0)] \tag{13}$$

where (σ_0, T_0, c_0) are reference values. Unfortunately, the dependence of $\tilde{\sigma}$ on temperature for even pure melts of important electronic materials is not known. The recent measurements of Hardy (1984) for silicon suggest that the form of Eq. 13 is appropriate for an extended range of T. The additional surface traction $\tilde{F}_s(x, t)$ is included in Eq. 11a to account for imposed stresses, such as the direct coupling of an electromagnetic field generated by a radio-frequency (RF) field, which leads to vigorous stirring of the melt. Including this effect as a surface force is a valid approximation for an electrically conducting melt and a high-frequency RF field (Sneyd, 1979).

A major complication in the analysis of convection and segregation in melt crystal growth is the need for simultaneous calculation of the melt/crystal interface shape with the temperature, velocity, and pressure fields. For low growth rates, where the assumption of local thermal equilibrium is valid, the shape of the solidification interface ∂D_{bI} is given by the shape of the liquidus curve $T_m(c)$ for the binary phase diagram, i.e.,

$$\tilde{T}(\tilde{x}, \tilde{t}) = T_m(c), \tilde{x} \in \partial D_{bI} \tag{14}$$

The influence of surface curvature and the surface free energy on the melting temperature has been neglected in this expression, because it is so small that it is unimportant in determining the macroscopic shape of the interface. However, microscopic details of melt/crystal interface structure, such as the onset of cellular and dendritic growth, depend crucially on the contribution of the surface energy to set the length scale of the pattern; this point is discussed further in the section on transport processes and solid microstructure. In addition to Eq. 14, latent heat is released at the melt/crystal interface and must be included in the interfacial energy balance.

Scaling Analysis. The complexity of practical crystal growth systems makes difficult the understanding of the roles of each of the driving forces for convection. As can be imagined from the expanded view of CZ growth shown in Figure 6, different driving forces—e.g., crystal and crucible rotation, buoyancy-driven and surface-tension driven flows—dominate the flow in different parts of the melt. The need for full numerical solutions that account for all these effects is clear. However, scaling analysis that balances the effects of various driving forces in idealized geometries has great utility for computing order-of-magnitude estimates of flow intensity and the scalings for changes in flow intensity with variations in boundary conditions and thermophysical properties. The results of such scaling analyses are described below.

The differential equations and boundary conditions are put in dimensionless form by introducing characteristic scales for the length, time, velocity, concentration, etc., that are picked to reflect the dominant mechanisms for transport in each conservation law. Then the dimensionless groups in the equations supply estimates for the relative magnitudes of various driving forces. Some of the dimensionless groups for convection and segregation in the melt are listed in Table 2 and are discussed below.

The Schmidt (Sc) and Prandtl (Pr) numbers, Table 2, are ratios of molecular diffusivities and thus are formed purely from thermophysical properties of the melt. Prandtl numbers relevant to melt crystal growth vary between the large values (1–10) for oxide melts to the extremely low values (0.01–0.1) for semiconductor melts. The Schmidt numbers are large (between 10 and 100) because of the low solute diffusivities for typical melts.

Examples of groups that specify ratios of transport mechanisms are listed next in Table 2 and depend on the size and shape of the domain. The Peclet numbers for heat (Pe_t) and solute (Pe_s), and momentum (Re) transport are ratios of scales for convective to diffusive transport and depend on the magnitudes of the velocity field and the length scale for the diffusion gra-

dient. Boundary layers form at large Peclet numbers, either Pe_t or Pe_s, or at large Re. The second possibility is particulary important in crystal growth from the melt, where the low values of solute diffusivity lead to convectively-dominated species transport, even at low fluid velocities. The choices for the velocity and gradient length scales in complex systems are not obvious, and different combinations are appropriate in different portions of the flow domain for real systems.

The next set of dimensionless groups listed in Table 2 scale the strength of a particular driving force for convection relative to the damping action of viscosity. The Rayleigh and Grashof numbers correspond to scaling the strength of buoyance-driven convection relative to viscosity and arise when different scales are used for velocity and pressure in the equation of motion. The Marangoni number (Ma) scales the magnitude of the surface shear stress due to a surface tension gradient to viscosity. The scale of the surface tension gradient has been taken as $(d\tilde{\sigma}/d\tilde{T})\,(d\tilde{T}/d\tilde{x})$ so only variations caused by temperature differences are taken into account.

The shape of the melt/fluid interface in a meniscus-defined crystal growth system is set by surface tension and gravitational force, and by viscous and dynamic pressure forces on the surface. The Bond number (hydrostatic pressure, Bo), capillary number (viscous stress, Ca) and Weber number (dynamic pressure, We) measure the magnitude of these forces scaled against surface tension. Most of the theoretical and numerical analyses of heat transfer and convection in meniscus-defined crystal growth discussed below are for idealized geometries where the meniscus is represented by a coordinate surface in a separable orthogonal coordinate system, e.g., a plane or a cylinder. The calculations assume that the underlying flow causes little deflection of the meniscus. This last assumption is mathematically equivalent to taking $Ca \ll 1$ and $We \ll 1$.

The Hartmann number (Ha) and the magnetic interaction parameter (N) are listed in Table 2 and scale the importance of an applied magnetic field to the action of viscosity and inertia, respectively. Treating the interaction of a magnetic field as a body force that introduces only the Lorentz force in Eq. 1 is an idealization valid when the melt is so electrically conductive that convection of charge by the flow is unimportant; i.e., when the Peclet number appropriate for electrical charge transport is small. This assumption is justified in most semiconductor melts and has been used in all the numerical computations reported thus far. The electromagnetic force generated by an RF induction heater directly coupled to a floating zone leads to a surface Hartman number that measures the effective surface force in the high-frequency limit. Muhlbauer et al. (1983) treat the effect of the RF field in numerical simulations of flow in a large-scale floating zone.

Analysis of flows in which more than one driving force exists has been limited to several idealized cases of thermosolutal convection driven by vertical and constant temperature and concen-

Table 2. Dimensionless Groups Appearing in Transport Equations for the Melt

Name	Meaning	Definition
Prandtl No.	$\frac{\text{Viscous diffusivity}}{\text{Heat diffusivity}}$	$Pr = \frac{\nu}{\alpha}$
Schmidt No.	$\frac{\text{Viscous diffusivity}}{\text{Species diffusivity}}$	$Sc \equiv \frac{\nu}{D}$
Thermal Peclet No.	$\frac{\text{Convective heat transport}}{\text{Diffusive heat transport}}$	$Pe_t \equiv \frac{V^*L^*}{\alpha}$
Solutal Peclet No.	$\frac{\text{Convective species transport}}{\text{Diffusive species transport}}$	$Pe_s \equiv \frac{V^*L^*}{D}$
Reynolds No.	$\frac{\text{Convective momentum transport}}{\text{Viscous momentum transport}}$	$Re \equiv \frac{V^*L^*}{\nu}$
Grashof No.	$\frac{\text{Buoyancy force}}{\text{Viscous force}}$	$Gr_t \equiv \frac{G\beta_T L^3}{\nu^2}\Delta T^*$
Rayleigh No.	$\frac{\text{Buoyancy force}}{\text{Viscous force}}$	$Ra_t \equiv Gr_t \cdot Pr$
Marangoni No.	$\frac{\text{Force due to surface tension gradient}}{\text{Viscous force}}$	$Ma_t \equiv \frac{\sigma(d\tilde{\sigma}/d\tilde{T})L}{\rho\nu^2}\Delta T^*$
Gravitational bond No.	$\frac{\text{Gravitational force on meniscus}}{\text{Surface tension force}}$	$Bo \equiv \frac{gL^{*2}}{\sigma_0}\Delta\rho$
Capillary No.	$\frac{\text{Viscous force on meniscus}}{\text{Surface tension force}}$	$Ca \equiv \frac{V^*\mu}{\sigma_0}$
Weber No.	$\frac{\text{Inertia force}}{\text{Surface tension Force}}$	$We \equiv \frac{\rho V^{*2}L^*}{\sigma_0}$
Hartmann No.	$\frac{\text{Lorentz force}}{\text{Viscous force}}$	$Ha \equiv B_0L^*\,(\sigma/\rho\nu)^{1/2}$
Magnetic Interaction parameter	$\frac{\text{Lorentz force}}{\text{Inertia force}}$	$N \equiv \frac{\sigma B_0^2 L^*}{\rho V^*}$

tration gradients. A discussion of thermosolutal convection is presented by Brown (1987a).

When the temperature and concentration gradients are perfectly vertical, thermosolutal convection begins at critical values of thermal or solutal Rayleigh numbers (Ra_t or Ra_s) as an instability from a static fluid. Increasing the driving force leads to finite-amplitude flows and to nonlinear transitions as discussed in the section on transport processes and defect formation. Surface-tension-driven motions also onset at a critical value of the Marangoni number when the free surface is perpendicular to a perfectly vertical temperature gradient (Pearson, 1958; Scriven and Sternling, 1964).

Imperfect alignment of the vertical gradient causes convection for any value of the driving force. The motion is weak for small values of the Grashof number (Gr) and represents a balance of viscous and buoyancy forces. Boundary layers form at higher values of Grashof number where viscous effects are confined to boundary and internal shear layers, and the core flows are set by a balance of inertia and buoyancy. Increasing the driving force in these flows also leads to transitions to time-periodic and chaotic convection.

The complexity of the temperature field in even the most carefully designed crystal growth systems leads to both vertical and horizontal temperature gradients in the melt, so that buoyancy-driven and surface-tension-driven flows are always present. Analysis of the flows in a slender rectangular cavity heated at the ends has been used as a test problem for flows driven by lateral temperature variations. Using the aspect ratio of the cavity as a perturbation parameter reduces the analysis to the solution of a sequence of problems in which the flow in the core of the cavity is dictated by an almost one-dimensional balance of buoyancy and viscous forces and the turning flows at the ends of the cavity are two-dimensional, but inertialess. The rigorous perturbation theory for this approach was introduced by Cormack et al. (1974) for two-dimensional buoyancy-driven motions and was extended by Hart (1983a, b) to include the stability of these motions for fluids with low Prandtl number. Hurle et al. (1974) have observed three-dimensional oscillatory flows in a slender cavity of gallium heated from the ends.

Similar analyses are available for surface-tension-driven flows in a slender cavity with the additional assumption that the meniscus at the top of the cavity is also flat (Sen and Davis, 1982). Smith and Davis (1982; 1983a, b) have used this configuration to study the stability of the flow with respect to wavelike instabilities; also see Davis (1987). Homsy and Meiburg (1984; also see Carpenter and Homsy, 1985) have analyzed the effect of a surface-active agent on the thermocapillary motion in a slender cavity.

Convection in the crystal growth systems discussed earlier cannot be characterized by analysis with either perfectly aligned vertical temperature gradients or slender cavities, but have spatially varying temperature fields and nearly unit aspect ratios. Even when only one driving force is present, such as buoyancy-driven convection, the flow structure can be quite complex and little insight into the nonlinear structure of the flow has been gained by asymptotic analysis.

Hjellming and Walker (1986, 1987a) and Langlois and Walker (1982) discovered an important exception to this situation that arises when a strong axial magnetic field is imposed on the melt. They analyzed the motion in a prototype of the Czochralski crystal growth system for the case in which the magnetic interaction parameter N and Hartmann number Ha are so large that fluid inertia can be neglected everywhere and viscous forces are confined to Hartmann layers, which are needed to satisfy no-slip and shear stress boundary conditions and to conserve mass between adjacent flow cells. The length scales for these Hartmann layers for rotational and buoyancy-driven flows are shown in Figure 7, which is taken from the analysis of Hjellming and Walker. The flow outside the boundary layers is determined by a balance of buoyancy and Lorentz forces. Moreover, the core flow can be written explicitly in terms of the temperature field. A self-consistent heat transfer problem is developed in the limit where the thermal Peclet number is small enough that temperature boundary layers are much thicker than the Hartmann layers.

Importance of Flow Transitions. Witt and his colleagues (K.M. Kim et al., 1972, 1978) documented the "microscopic changes" in crystal growth rate and axial solute segregation caused by short time scale variations in the temperature and velocity fields. They did this by perfecting the use of Peltier interface demarcation (Singh et al., 1968; Witt et al., 1983); a good description of this technique is given by Wargo and Witt (1984). Here current pulses are passed through the melt and crystal at regular intervals so that the Peltier effect causes periodic local cooling of the melt/crystal interface and leads to rapid, but small, changes in the local freezing rate. These changes in the microscopic solidification rate result in layers of high solute incorporation, which can be detected optically in a polished and etched sample sliced along the growth axis. Pictures of the etching patterns taken from a vertical Bridgman experiment with melt below the crystal are shown in Figure 8 for the growth of gallium-doped germanium (Kim et al., 1972). The picture in Figure 8d is the etching pattern introduced solely by the periodic Peltier pulses used to impart a time record in the crystal.

The pictures are taken at varying times during the translation of the ampoule through the furnace and so correspond to dif-

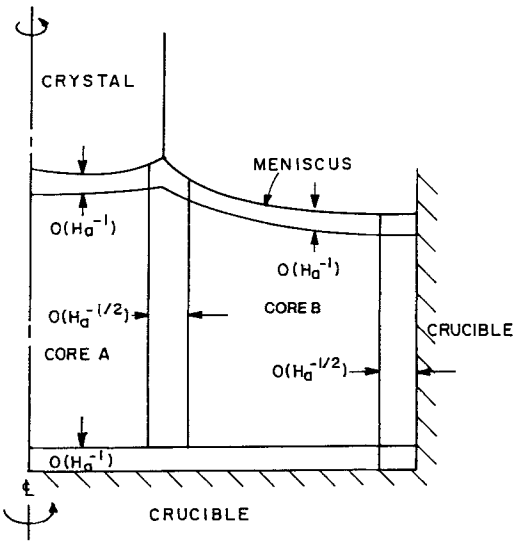

Figure 7. Regions of buoyancy-driven flow for CZ growth in a high axial magnetic field.
After results of Hjellming and Walker (1986)

ferent lengths of melt. The intensity of the convection scales with the thermal Rayleigh number for the vertical cylinder:

$$Ra_t \equiv \rho_0 \beta g L^3 \Delta T / \alpha v \qquad (15)$$

where ΔT is the temperature difference between the melting point and the hot end of the ampoule and L is the length of the melt. The length of the melt and Ra_t decrease from Figure 8a to Figure 8d is the etching pattern introduced solely by the periodic periodic markers in Figure 8a indicate aperiodic or chaotic convection at the highest convection level. Decreasing Ra_t reduces the convection to simply periodic behavior, as shown by the set of periodic striations superimposed on the marking pattern in Figures 8b and 8c. The disappearance of all striations other than the current-induced markings in Figure 8d is indicative of laminar convection in the melt. The frequency of the convective oscillations is a few tenths of a Hertz. The interpretations of the etching patterns given above is substantiated by the temperature measurements from a thermocouple in the melt during the same experiment; the transitions from a chaotic, to periodic, and finally steady or laminar temperature measurement are shown alongside the etching patterns in Figure 8.

Transitions from steady state to time-dependent surface-tension-driven motions are also well known and are important in meniscus-defined crystal growth systems. For example, the experiments of Preisser et al. (1982) indicate the development of an azimuthal traveling wave on the axisymmetric base flow in a small-scale floating zone.

Predicting these flow transitions and designing systems that suppress the onset of time-dependent motion are central to the controlled growth of compositionally uniform crystals. Although many theoretical and experimental studies exist that

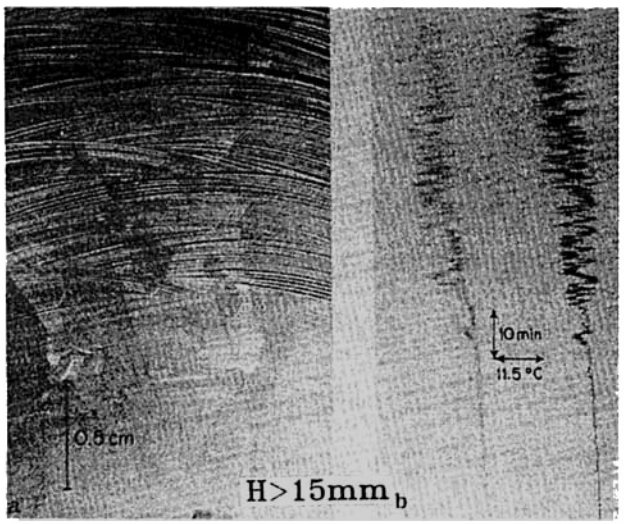

Figure 8a. Irregular pattern caused by chaotic convection.

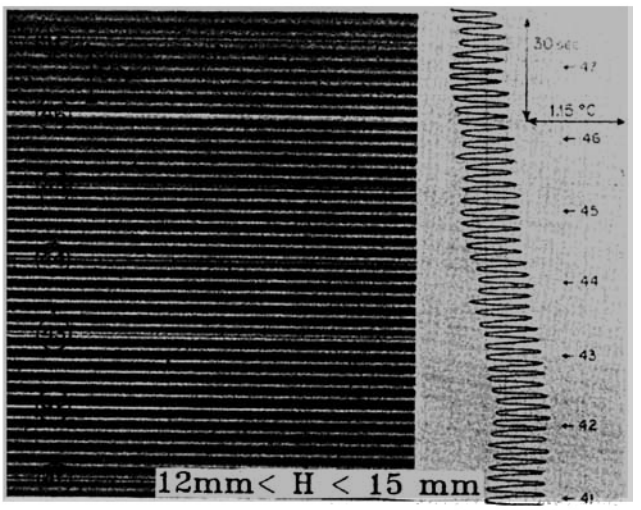

Figure 8b. Regular pattern caused by time-periodic convection.

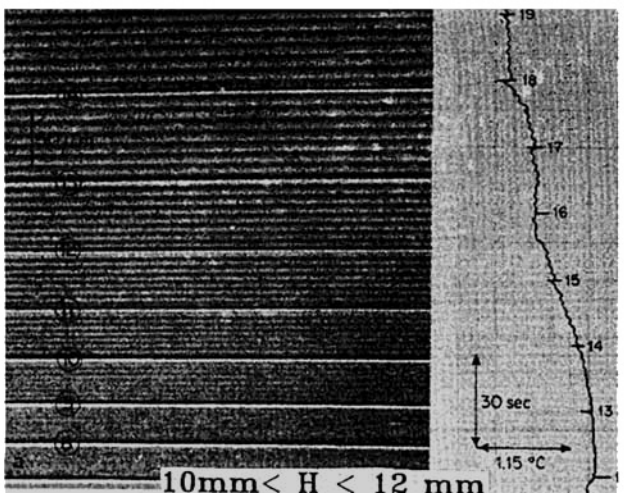

Figure 8c. Regular pattern caused by time-periodic convection.

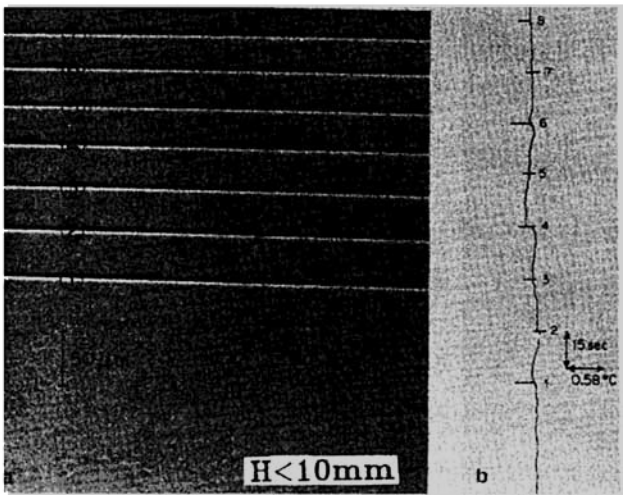

Figure 8d. Regular pattern due to Peltier pulses are used to mark growth rate of crystal.

Figure 8. Striation patterns revealed by etching Ga-doped InSb crystal.

Crystal grown in vertical unstable Bridgman system (Kim et al., 1972); transitions are caused by decreasing length of melt during growth of one crystal Temperature measurements made by a thermocouple in melt during crystal growth are shown alongside the etchings.

treat such transitions in idealized flow problems, the relevance of these results to crystal growth systems is limited; see Carruthers (1976, 1977) for comprehensive reviews. Direct prediction of the transitions in crystal growth systems is needed and is at the leading edge of current experimental and numerical analysis. Analysis of the transitions leading to chaotic convection in crystal growth experiments seems beyond present capabilities because of the three-dimensional nature of these flows and because of the sensitivity of the transitions following the onset of time-periodic motion to the details of the experimental system; for an example of this sensitivity see Abernathy and Rosenberger (1985). Moreover, the oscillations in the melt lead to tremendously disparate time scales for transport, ranging from the short temporal wavelength for the convective oscillations (~1 s) to the long time scale for growth ($\sim 1 \times 10^4$ s) to grow one cm of crystal at a rate of 10 μm/s.

Fortunately, the onset of oscillatory flow from a steady flow occurs as a Hopf bifurcation (Guckenheimer and Holmes, 1983) and is much more reproducible experimentally. Also, the existence of a Hopf bifurcation with increasing flow intensity can be detected in large-scale numerical calculations by solution of the equation set for the linear stability of the underlying laminar flow. This approach has been used in investigations of buoyancy-driven convection in idealized geometries (McLaughlin and Orszag, 1982; Curry et al., 1984; Sackinger et al., 1988a). Crochet and coworkers have studied the oscillations in the convection of a prototype of the horizontal Bridgman method for two-dimensional motion without (Crochet et al., 1983; 1987a) and including (Wouters et al., 1987) the melt/crystal interface. Crochet et al. (1987b) computed three-dimensional motions by direct simulation of the nonlinear, time-dependent equations. Winters (1987) has used computer-implemented perturbation methods for locating Hopf bifurcations to detect the onset of two-dimensional oscillations in the same system.

An important result of the understanding of transitions in buoyancy-driven convection in melt growth is the quantitative development of mechanisms for suppressing them. Applied magnetic fields have been shown experimentally by many research groups to be effective in laminarizing the flows in metallic melts (Utech and Flemings, 1966; Kim, 1982). The temperature measured as a function of time in a vertical Bridgman system with increasing intensity B of a transverse applied magnetic field by Kim (1982) is shown in Figure 9. The temporal structure varies from an aperiodic recording without the field, through time-periodic, and finally a steady state trace for increasing B. These transitions have not been predicted theoretically. Only a few numerical calculations (Langlois, 1984; Mihelcic and Winegrath, 1985) give an indication of the effect of field intensity on the transition to time-periodic motion. Comprehensive theoretical and numerical analyses of the interaction of the applied fields with the flow have been limited to the large field strengths that lead to laminar flows; these results are described above.

Models for influence of melt convection on solute segregation

Convection in the melt causes mixing of solutes and alters the diffusion layer adjacent to the melt/crystal interface. The spatial structure and intensity of the flow sets the axial (along the growth direction) and lateral (perpendicular to the growth direction) profiles of solute concentration in the crystal. The different regimes for solute segregation are shown in Figure 10 in terms of the uniformity of the solute concentration across the crystal Δc, which is defined as the maximum difference in the concentration across the crystal divided by the average value, $<\tilde{c}>_I$, and by the effective segregation coefficient k_{eff}, defined as

$$k_{eff} \equiv k \ll\tilde{c}\gg / <\tilde{c}>_I \tag{16}$$

where $\ll c\gg$ is the volume averaged concentration of solute in the melt.

These measures of solute segregation are closely related to the spatial and temporal pattern of the flow in the melt. Most of the theories discussed below are appropriate for laminar convection of varying strength and spatial structure. Intense laminar convection is rarely seen in the low Prandtl number melts typical of semiconductor materials. Instead, nonlinear flow transitions usually lead to time-periodic and chaotic fluctuations in the velocity and temperature field and induce melting and accelerated crystal growth on the typically short [0(1 s)] time scale of the fluctuations.

In diffusion-controlled directional solidification, the only velocity present in the melt is due to solidification. When the melt/crystal interface is planar this combination of diffusion and con-

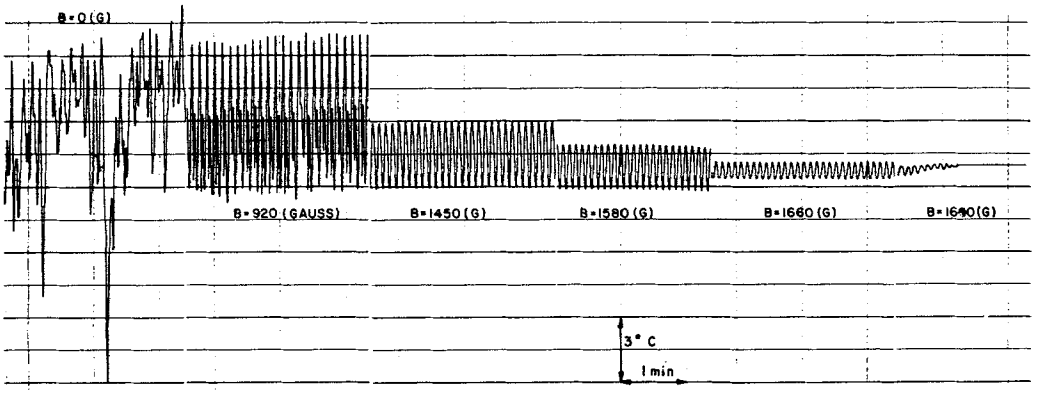

Figure 9. Thermocouple measurement as a function of time with increasing strength of an applied transverse magnetic field.

Results in a vertical Bridgman growth system (Kim, 1982); oscillations are damped by the field

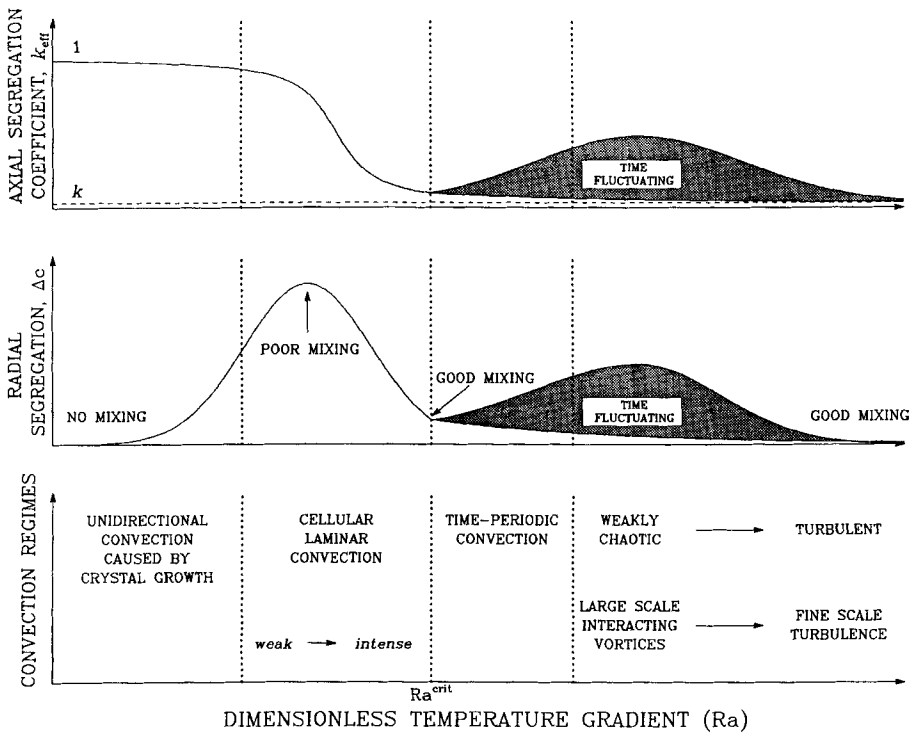

Figure 10. Regimes of solute transport in melt crystal growth.
Representation in terms of effects on radial segration Δc and effective segregation coefficient k_{eff}

vection leads to a uniform radial distribution of solutes, i.e., $\Delta c = 0$ and k_{eff} approaches unity, if the melt is sufficiently long that the diffusion layer next to the interface occupies only a small fraction of the length of the melt. Introducing cellular convection in the melt causes distortion of the diffusion-controlled profile, Eq. 4, independent of lateral concentration gradients due to curvature of the melt/crystal interface (Coriell and Sekerka, 1979; Coriell et al., 1981). Harriott and Brown (1984) demonstrated this mixing for flows driven by rotating the feed rod and crystal in small-scale floating zones in the limit where the Peclet number Pe_s based on the bulk velocity is small. The degree of radial nonuniformity is maximum for some intermediate level of convection. Increasing the intensity beyond this value causes homogenization of the melt and reduces the lateral segregation, $\Delta c \rightarrow 0$.

Convection also forces k_{eff} to approach k because the bulk concentration $\ll\bar{c}\gg$ is increased (assuming $k < 1$) due to the mixing of the diffusion layer with the melt in the remainder of the ampoule. In the limit of very intense convection, the variation in the concentration is confined to a boundary layer much thinner than D/V_g. Scheil (1942) first described axial segregation in the limit of complete mixing where the boundary layer thickness approaches zero.

The fluctuations in the velocity and temperature fields caused by time-periodic or chaotic flows lead to fluctuations in the axial and radial segregation of solute, as indicated by the final region in Figure 10. The etching patterns in Figure 8 are the best experimental indication of the temporal characteristics of the convection and have been used as a guide to the analysis of the effect of magnetic fields on convection by Robertson and O'Connor (1985) for large-scale floating zone experiments. Relating the frequency response of the axial composition profile directly to the characteristics of the chaotic flow is complicated by the melting and accelerated growth of the crystal due to the concomitant fluctuations in the temperature field.

Solute segregation with bulk convection is given rigorously by solution of the two-dimensional solute balance equation [for a two-dimensional velocity field $v(r, z)$], written here in the dimensionless form of Eq. 8:

$$Pe_s\,(\partial c/\partial t + \boldsymbol{v} \cdot \nabla c) = \nabla^2 c \tag{17}$$

where $Pe_s \equiv V_0 L/D$ is the Peclet number for mass transfer defined in Table 2 and scales the importance of convective solute transport by the velocity in the bulk (scaled by V_0) to diffusion. The dimensionless solute balance at the melt/crystal interface is the generalization of Eqs. 3 for a steadily solidifying interface ∂D_I:

$$\boldsymbol{n} \cdot \nabla c = Pe_g c(1 - k)\boldsymbol{n} \cdot \boldsymbol{e}_g, \text{ at } \partial D_I \tag{18}$$

where $\boldsymbol{n}$ is the unit normal to the melt/crystal interface, $\boldsymbol{e}_g$ is the unit vector in the direction of crystal growth, and $Pe_g \equiv V_g L/D$ is the dimensionless crystal growth rate, or alternatively, the Peclet number based on the solidification velocity. The appropriate boundary conditions along the other surfaces depend on the geometry of the system and the chemical interactions of these boundaries with the melt. For many melts, ampoule and crucible materials are inert and these surfaces correspond to no-flux boundaries for solutes. Chemical interactions are important in some systems. For example, the quartz crucibles used in silicon growth dissolve when contacted with the melt and modeling of oxygen incorporation in the crystal must account for this flux in addition to the losses of oxygen to the ambient that occur in

meniscus-defined growth (Carlberg et al., 1982; Murgai, 1985).

The Stagnant Film. The concept of a stagnant film thickness, as proposed by Nernst (1904), is the most widely used characterization of the role of convection in solute segregation in crystal growth. This application was reviewed by Wilcox (1969). As shown in Figure 11, convective mixing is assumed to be totally effective outside of a thin layer adjacent to the melt/crystal interface in which species transport is only by diffusion and the melt motion caused by solidification. If the composition of solute in the bulk ($\tilde{z} > \tilde{\delta}$) is c_0, the steady state composition profile in the layer is derived by solving Eqs. 2 and 3 with the boundary condition

$$\tilde{c}(\tilde{\delta}) = c_0 \tag{19}$$

This yields

$$\frac{\tilde{c}(\tilde{z})}{c_0} = \frac{k + (1 - k)\exp(-V_g\tilde{z}/D)}{k + (1 - k)\exp(-V_g\tilde{\delta}/D)} \tag{20}$$

as originally given by Burton et al. (1953).

The effective segregation coefficient k_{eff} is defined in terms of the stagnant film thickness as

$$k_{eff} \equiv \frac{k}{k + (1 - k)\exp(-V_g\tilde{\delta}/D)} \tag{21}$$

Expression 21 is the most often used relation for correlating axial segregation data from experiment and is amazingly successful for this purpose. It is rewritten for a finite-length ampoule in terms of the fraction f of the sample solidified to give the normal freezing expression

$$\frac{\tilde{c}_s}{c_0} = k_{eff}(1 - f)^{(k_{eff}-1)} \tag{22}$$

for the composition of the crystal $\tilde{c}_s = k\tilde{c}_m$ grown from a melt with initial composition c_0. Figure 12 shows a sample profile from the growth of gallium-doped germanium by Wang (1984), which fits Eq. 21 with an equilibrium segregation coefficient $k = 0.087$ and k_{eff} between 0.09 and 0.11.

Although the notion of a stagnant film is a useful concept for thinking about the role of convection in axial solute segregation, it has well-known deficiencies (Wilcox, 1969) that prevent it from being predictive. Stagnant film theory is formulated as if mixing is perfect outside of the stagnant film and bulk convection does not modify the velocity field inside the layer. These assumptions prevent the prediction of changes in axial segregation (k_{eff}) caused by changes in the intensity of the flow without additional empirical correlation for $\tilde{\delta}$ as a function of convection from either experimental (Burton et al., 1953a, b; Zief and Wilcox, 1967) or computational (Adornato and Brown, 1987a, b) data for the effective segregation coefficient and Eq. 21. Also, because the velocity field in the stagnant film is assumed to correspond only to the growth rate, the stagnant film model gives no prediction of the concentration variations along the crystal surface caused by lateral nonuniformities in the flow.

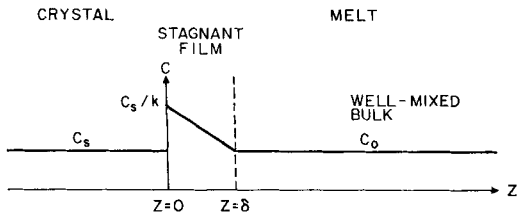

Figure 11. Stagnant film in solute transport in melt growth.

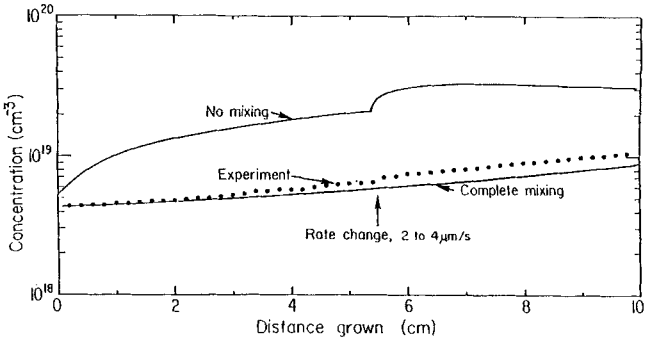

Figure 12. Axial segregation data for growth of Ga-doped Ge in a vertical Bridgman furnace.
From Wang (1984)

Analysis of the Solute Boundary Layer. Closed form solution of the species balance, Eq. 7, with the interfacial balance, Eq. 8, and the condition that $\tilde{c} \to c_0$ as $\tilde{z} \to \infty$ is only feasible when either convection contributes only weakly to transport, as was the case in the analysis of Harriott and Brown (1984), or when the variation of the concentration from unity is confined to a boundary layer adjacent to the growing crystal. Burton et al. (1953b) analyzed the specific case of solute segregation near a rotating crystal, as occurs in CZ growth. The velocity field near the crystal was taken to be the sum of a uniform crystal growth rate V_g and the self-similar axisymmetric velocity field due to rotation of an infinitely large crystal surface, as described by the asymptotic expansion of Cochran (1934).

Because the axial velocity is independent of radial distance from the center of the crystal, the concentration field varies only axially and is given by the solution of the solute balance equation with the approximate velocity field of the form

$$\tilde{v}_z = -V_g - V_0(\tilde{z}^2/L^2) \tag{23}$$

where L is a characteristic length scale for the bulk flow ($L^2 \equiv \nu/\Omega$; Ω is the angular velocity of the disk in the similarity solution of Cochran, 1934, and $V_0 \equiv \Omega R$ is the rotational velocity of the crystal. The closed-form solution of this problem is written in terms of exponential integrals, as described in (Burton et al., 1953b). The effective segregation coefficient is expressed analogously to Eq. 21 as

$$k_{eff} = \frac{k}{k + (1 - k)\exp(-\Delta)} \tag{24}$$

where the constant Δ is defined as

$$\Delta \equiv -\ln\left\{1 - \int_0^\infty \exp[-(\xi + \lambda\xi^3)]\,d\xi\right\} \tag{25}$$

and $\lambda \equiv (V_0/3V_g)$ is the ratio of the components of the velocity field due to the bulk flow and to solidification.

Wilson (1978a, b) has pointed out that Δ is *not* the dimensionless thickness of the diffusion boundary layer scaled with D/V_g, as originally suggested by Burton et al. (1953b), except in the limit where the velocity field in the layer is dominated by the bulk flow, i.e., $\lambda \gg 1$. In this case the analysis reduces to the one presented first by Levich (1962) and the integral in Eq. 25 is approximated as

$$\Delta \simeq \Gamma(1/3)\,\lambda^{-1/3}/3, \lambda \gg 1 \tag{26}$$

where $\Gamma(\cdot)$ is the gamma function. When the ratio λ is rewritten in terms of the Peclet numbers $Pe_s \equiv V_0 L/D$ and $Pe_g \equiv V_g L/D$ as $\lambda = (Pe_s/3Pe_g)$, the scaling in Eq. 26 is recognized as the scaling for a boundary layer adjacent to a no-slip surface. In the limit where the solidification rate dominates ($\lambda \ll 1$) the boundary layer is controlled by a balance of diffusion and convection caused by the solidification velocity; then Δ scales as Pe_g^{-1}.

Wilson (1978b) defined a conventional boundary layer thickness $\tilde{\Delta}$ as

$$\tilde{\Delta} \equiv \frac{\tilde{c}(0) - c_0}{[-d\tilde{c}/d\tilde{z}(0)]}\left(\frac{V_g}{D}\right) = 1 - \exp(\Delta) \tag{27}$$

The constant $\tilde{\Delta} \simeq \Delta$ in the limit $\lambda \to \infty$, because Δ is small. Then the boundary layer thickness is expected to vary according to Eq. 26.

The boundary layer structure predicted by the analysis of Burton et al. (1953b) and by Wilson is much more robust than just a description of the solute boundary layer caused by the rotational flow near a large crystal. When a stagnation flow on the melt/crystal interface is created by any mechanism and is intense enough to lead to a thin solute boundary layer, the velocity field in the boundary layer can be described by

$$\tilde{v}_z(\tilde{r}, \tilde{z}) = -V_g - V_0 \underline{F(\tilde{r})}\tilde{z}^2 \tag{28}$$

where V_0 sets the scale of the bulk convection and the variation in the lateral direction $F = F(\tilde{r})$ is slow compared to the rapid variation in the perpendicular direction $\tilde{z}$. Then the local concentration field, the effective segregation coefficient, and lateral solute uniformity follow directly from the analysis described above. Assuming that $Pe_s \equiv V_0 L/D \gg 1$ and $Pe_g \equiv V_g L/D = 0(1)$ leads to a dimensionless boundary layer equation valid away from the edges of the crystal:

$$2\eta \frac{\partial c}{\partial r}\int_0^r F(u)\,du - F(r)\eta^2 \frac{\partial c}{\partial \eta} = \frac{\partial^2 c}{\partial \eta^2} + O(Pe_s^{-2/3}) \tag{29}$$

where $\eta \equiv zPe_s^{-1/3}$ is the stretched coordinate in the boundary layer and $(r, z) \equiv (\tilde{r}/L, \tilde{z}/L)$. The concentration is assumed to scale with a bulk value of c_0. The scaled form of the solute balance at the interface is

$$\left.\frac{\partial c}{\partial \eta}\right|_{\eta=0} = -Pe_g \cdot Pe_s^{-1/3}(1-k)\,c(r, 0) \tag{30}$$

Techniques from boundary layer analysis can be used to construct a series solution to Eqs. 29 and 30 of the form

$$c(r, \eta) = 1 + C_1(r, \eta)\,Pe_s^{-1/3} + O(Pe_s^{-2/3}) \tag{31}$$

This result is the same as the structure of a concentration boundary layer adjacent to a no-slip boundary (Pan and Acrivos, 1968), which is implied by the form of Eq. 28 and conservation of mass. This structure has been seen in concentration fields computed numerically for highly convected melts; see the work of Harriott and Brown (1984) and Adornato and Brown (1987a, b). Camel and Favier (1986) predicted the same scaling for the radial segregation across the interface and the effective segregation coefficient from an order-of-magnitude analysis that corresponds to the scalings described here.

The multicellular structure of laminar convection in small-scale crystal growth systems complicates the interpretation of the boundary layer analysis because the almost constant level of the concentration field in each cell is unknown *a priori* and each cell communicates with its neighbors by diffusion through thin internal layers that separate them. These bulk concentrations also scale with Pe_s. Examples of multicellular structures are shown in the finite-element calculations of Harriott and Brown (1984) for small-scale floating zones and the analysis of Adornato and Brown (1987a, b) for directional solidification. This later work is reviewed in the section below on vertical Bridgman-Stockbarger crystal growth.

Several groups (Series et al., 1985; Hurle and Series, 1985; Cartwright et al., 1985) have extended the similarity analysis of Burton et al. (1953b) to the case where an axial magnetic field is imposed on the melt with sufficient strength that $Ha \gg 1$ and $N \ll 1$. In this limit a closed-form asymptotic expression exists that describes the variation in the flow field across the thin $O(Ha^{-1})$ Hartmann layer adjacent to the disk. Axial solute segregation across this layer was analyzed by assuming that the melt outside of the Hartmann layers is well mixed. The effective segregation coefficient approaches one when the field strength is increased, as expected for any mechanism that damps convection near the crystal.

Hjellming and Walker (1987b) have presented a semiquantitative analysis of solute transfer with a strong magnetic field for an entire Czochralski system by coupling the asymptotic analysis of the flow and temperature fields described in previously with boundary layer models for solute transport across the Hartmann layers caused by the field. An important conclusion of this analysis is that the solute transfer for typical magnetic field strength will be transient throughout the entire crystal growth run, because of the long diffusion time necessary for the species to traverse the Hartmann layers.

Connection between transport processes and solid microstructure

The formation of cellular and dendritic patterns in the microstructure of binary crystals grown by directional solidification results from interactions of the temperature and concentration fields with the shape of the melt/crystal interface. Tiller et al. (1953) first described the mechanism for "constitutional supercooling" or the microscale instability of a planar melt/crystal interface toward the formation of cells and dendrites. We repeat their description for a simple system with a constant tempera-

ture gradient G (K/cm) and a melt that moves only to account for the solidification rate V_g. If the bulk composition of solute is c_0 and the solidification is at steady state, the exponential diffusion layer forms in front of the interface. The elevated concentration (assuming $k < 1$) in this layer corresponds to melt that solidifies at a lower temperature given by the phase diagram, Figure 5, as

$$\tilde{T}_m = \tilde{T}_m^0 + \tilde{m}\,\tilde{c} \tag{32}$$

where $\tilde{m} < 0$, and $\tilde{T}_m^0$ is the melting temperature of the pure material. The melt in the diffusion layer should solidify at a higher temperature than the value at the interface ($\tilde{T}_m^0 + \tilde{m}c_0/k$). If the temperature gradient $\tilde{G}$ is low enough the melt in front of the interface may be supercooled so that any small protuberance of the solid will solidify.

Tiller et al. (1953) derived a criterion for the onset of this instability by estimating the rate of change of the melting temperature of the melt in front of the interface as $\tilde{m} \cdot (d\tilde{c}/c\tilde{z})_l$ and evaluating the gradient from the solute balance at the interface, Eq. 4. The criterion for stability of the interface is that the actual temperature gradient must be larger than this value or

$$(\tilde{G}/V_g) > -\tilde{m}(c_0/Dk)\,(1-k) \tag{33}$$

Either decreasing the temperature gradient, increasing the concentration of solute, or increasing the growth rate leads to instability of the planar interface.

Although Eq. 33 gives a physical description for the mechanism of the instability that leads to microstructure formation during solidification, it is not rigorous because it does not take into account the effects of the rates of heat and species transport on the evolution of the disturbance, and because of this deficiency it cannot be used as a basis for further analysis of microstructure formation. This deficiency is clearest from the lack of a prediction of the spatial wavelength of the microstructure formed along the interface.

The spatial microstructure of the interface is strongly influenced by its surface energy, which appears in the Gibbs-Thomson equation (Woodruff, 1973) for the melting temperature of a curved interface

$$\tilde{T}_m = \tilde{T}_m^0 + \tilde{m}\tilde{c} + \tilde{\Gamma}(2\tilde{H}) \tag{34}$$

where $\tilde{\Gamma} \equiv \gamma/\Delta H_f$ is the capillary length associated with the surface energy γ, ΔH_f is the heat of fusion, and $\tilde{H}$ is the local mean curvature of the solidification front, defined so that $\tilde{H} > 0$ for an interface that is convex with respect to the crystal. Equation 24 implies that the melting point is increased by capillarity for short-wavelength disturbances ($H \gg 1$). This compensates for the constitutional supercooling mechanism, thereby implying a short-wavelength cutoff to the instability.

Mullins and Sekerka (1963, 1964) analyzed the stability of a planar solidification interface to small disturbances by rigorous solution of the equations for species and heat transport in melt and crystal and the constraint of equilibrium thermodynamics at the interface. For two-dimensional solidification samples in a constant temperature gradient, the results predict the onset of a sinusoidal interfacial instability with a wavelength $\tilde{\lambda}$ corresponding to the disturbance that is just marginally stable as either $\tilde{G}$ is decreased or V_g is increased. The following discussion focuses on considering the growth rate as the control parameter for transitions in the interface morphology.

The curves of neutral stability [$V_g = V_c(\tilde{\lambda})$] correspond to disturbances that become unstable for any further increase in the growth rate. Figure 13 shows a sample set of neutral stability curves for the succinonitrile-acetone alloy for a range of concentrations of acetone. The combination of succinonitrile and acetone is a well-characterized organic alloy used extensively in experiments simulating metal solidification (Glicksman et al., 1986). Several features of these curves are universal. First, the curves are closed; a disturbance with a particular wavelength $\tilde{\lambda}$ becomes unstable at a critical growth rate $V_c(\tilde{\lambda})$, but is restabilized at the higher growth rate corresponding to the top section of the curve. Second, decreasing the concentration of the solute decreases the size of the region of unstable wavelengths, as expected from the constitutional supercooling criterion.

Although the balance equations are linear, in the absence of bulk convection, the unknown shape of the melt/crystal interface and the dependence of the melting temperature on the energy and curvature of the surface make the model for microscopic interface shape rich in nonlinear structure. For a particular value of the spatial wavelength, a family of cellular interfaces evolves from the critical growth rate $V_c(\tilde{\lambda})$ when the velocity is increased. The evolution of these cellular forms to deep cells and dendrites with increasing V_g is governed by the full nonlinear equations. Figure 14 contains pictures of the cell-to-dendrite transition with increasing growth rate in a thin solidification sample for succinonitrile-acetone (Trivedi and Somboonsuk, 1984). Figure 14a shows shallow cells, which develop deep grooves, Figure 14b, and finally dendritic sidearms, Figure 14c, as the growth rate is increased; even in the thin sample the dendritic structures are not two-dimensional, as indicated by the sidearms that protrude out of the plane of the photograph.

Prediction of these nonlinear transitions, especially the spatial wavelength of the microstructures, is an active area of research. Full numerical solution of nonlinear models for microscopic solidification (Ungar and Brown, 1984; Ungar et al., 1985; Bennett et al., 1988) have shown the development of deep cells for ranges of spatial wavelengths within the unstable region of the

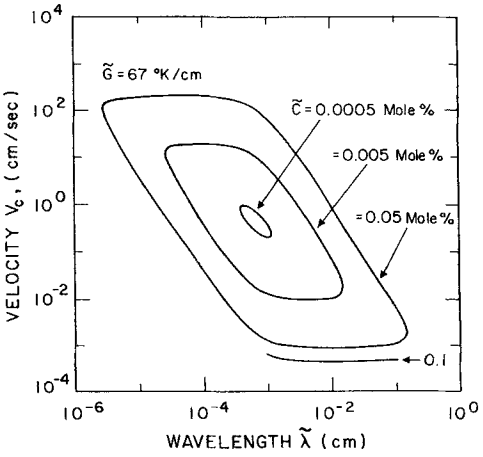

Figure 13. Neutral stability curves computed by linear analysis for succinonitrile-acetone system as a function of acetone concentration.

Fixed temperature gradient, G = 67°/cm

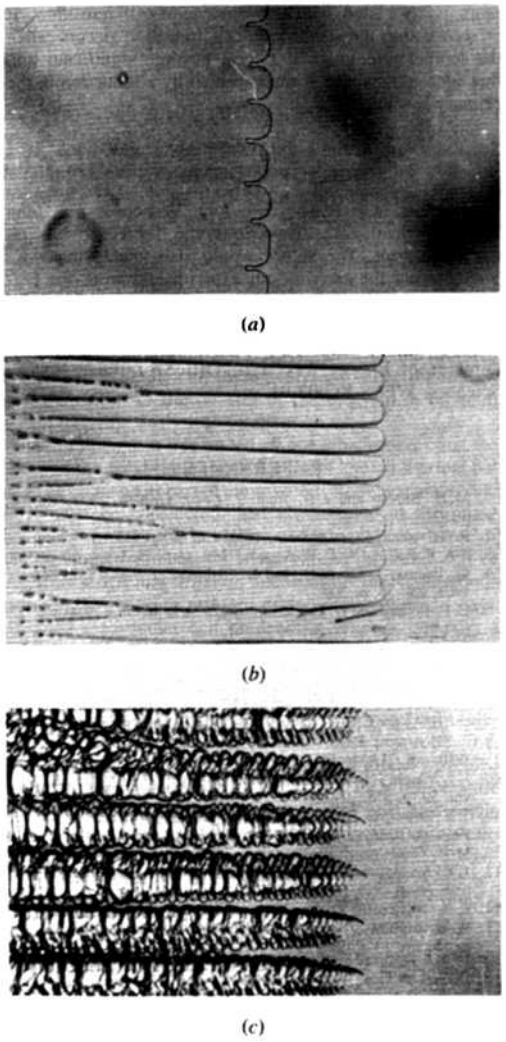

Figure 14. Cellular and dendritic structures in a thin-film solidification experiment.
Results using succinonitrile-acetone (Trivedi and Somboonsuk, 1984)

neutral stability curve and have demonstrated mechanisms for splitting on individual cells (cell birth) and for merging of cell pairs (cell death). Dynamical calculations indicate that there may be no mechanism for wavelength selection in collections of shallow cells (Brown et al., 1987). Deep cells, like those in Figure 14b, have been computed as the growth rate is increased (Ungar and Brown, 1985). These cells exist for ranges of wavelength and have rounded tips connected to slender sidewalls leading to a cell root with a smooth bottom. Recent asymptotic (Langer and Hong, 1986) and numerical calculations (Karma, 1986) suggest that a wavelength selection mechanism may exist when the bottom of the cell is not present and the surface energy is vanishingly small.

Including bulk convection in the models describing interface microstructure severely complicates the analysis. The current state of research in this area is reviewed by Glicksman et al. (1986). Several analyses demonstrate that novel interactions between the local flow and the interface morphology are possible when the two phenomena are coupled (Coriell et al., 1980; Davis et al., 1984).

Connection between transport processes and defect formation in the crystal

Analysis of the connection between macroscopic transport processes in the melt and crystal, e.g., the temperature field in both phases and solute transport near the melt/crystal interface, and defects in the crystal requires understanding of the mechanisms for the generation (in the bulk crystal and at the interface), motion, combination, multiplication, and annihilation of crystallographic defects and dislocations. Description of this coupling for crystal growth has been confined to the simple picture from continuum thermoelasticity for a perfect crystal where temperature gradients in the crystal during processing create stress in the solid which causes dislocations when its magnitude exceeds the critical resolved shear stress (CRSS) evaluated in the slip directions for the crystal. Billig (1956) introduced this notion to explain the generation of dislocations in germanium crystals grown by the Czochralski (CZ) method. Several authors have used this idea to develop qualitative estimates for the bounds on temperature gradients in CZ growth. Tsavinsky (1979) estimated the maximum diameter crystal that can be grown before the CRSS is reached. Brice (1976) found a relationship between the magnitude of the shear stress in the solid and crack formation.

Jordan et al. (1980) refined the thermoelastic stress calculation for the analysis of the spatial distribution of dislocations in GaAs grown with the liquid-encapsulated CZ (LEC) method. Their analysis was based on a two-dimensional model for the temperature field throughout the grown crystal that included all of the critical parameters, e.g., pull rate, heat transfer between the crystal, and the ambient and thermophysical properties. In this and in other related works (Jordan et al., 1981; Duseaux, 1983; Kobayashi and Iwaki, 1985), the crystal was assumed to be an isotropic material with a constant coefficient of expansion, so that the strains in the material are only functions of the local axial and radial temperature gradients. Then nonconstant displacements of the crystal, which lead to nonisotropic stress in the solid, are caused by nonconstant temperature gradients.

Jordan calculated these strains in closed form by assuming that only deformations in the azimuthal plane of the crystal are important. Duseaux (1983) and Kobayashi and Iwaki (1985) considered both radial and axial displacements by numerically calculating the strains. Figure 15 shows a direct comparison between the magnitude of the shear stress predicted by the analysis of Jordan et al. (1980) and the pattern of dislocations in a GaAs crystal grown by the LEC technique. Although a quantitative comparison is not meaningful, the similar patterns for regions of high stress and high dislocation density near the edge of the crystal are very suggestive that thermoelastic stress plays an important role in dislocation formation.

The importance of the thermal conductivity of the crystal and the CRSS in determining the "degree of difficulty" for growing a specific material from the melt is understood in terms of the relationship between these parameters and the formation of dislocations in the crystal due to excess stress. Clearly materials with lower values of the CRSS must be grown in systems with lower temperature gradients to prevent crystallographic slip. Low values of the conductivity make this difficult to achieve.

The isoelectronic doping of GaAs crystals with indium introduced by Mil'vidskii et al. (1981; also see Jacob, 1982; Fornari et al., 1983; McGuigan et al., 1986) was based on the idea that

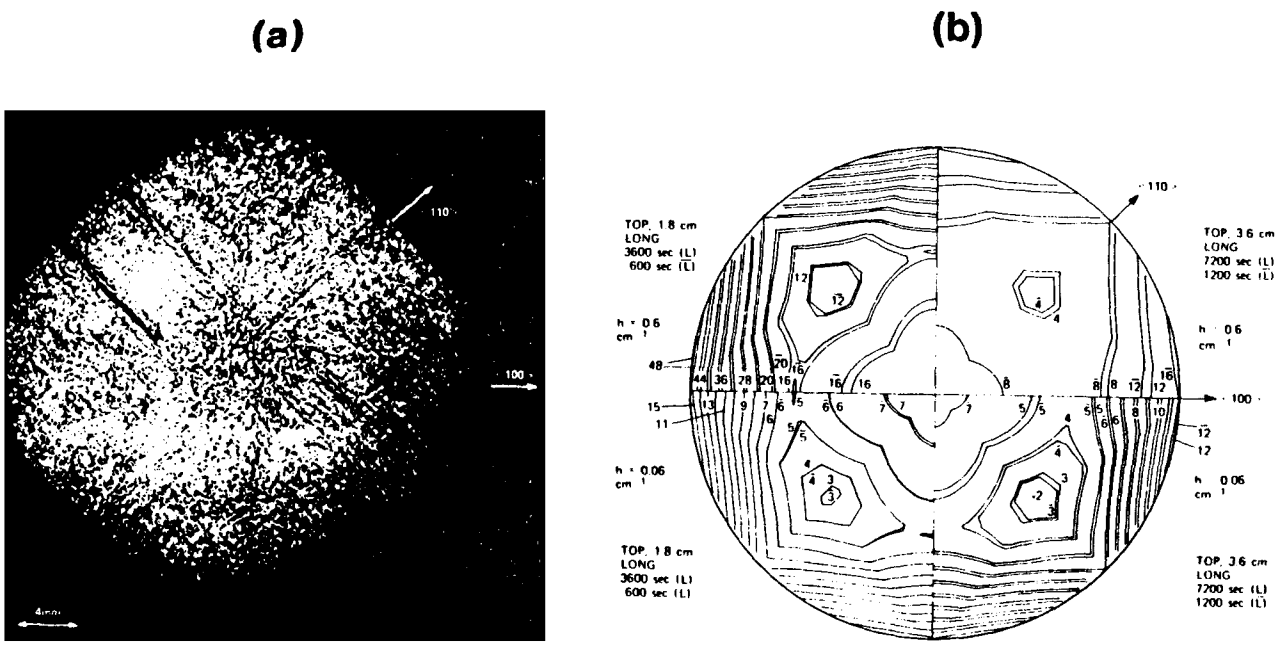

Figure 15. Comparison of measured dislocation density in GaAs wafer grown by LEC method with thermoelastic stress calculation (Jordan et al., 1980); (a) experimentally observed dislocation pattern; (b) contours of thermoelastic stress predicted by simulation. The high dislocation density around the periphery of the crystal is predicted by the calculations.

indium causes solid solution hardening of the GaAs lattice and raises the CRSS. Crystals with low dislocation densities have been grown by many groups using this method. Recent measurements of the value of the CRSS as a function of temperature and indium concentration (Tabache et al., 1986; Guruswamy et al., 1987) reveal a factor of two increase in CRSS in the temperature range just below the melting point. This difference is adequate to eliminate profuse dislocation multiplication in moderate-diameter crystals, but dislocation formation in crystals grown in a low stress environment remain unexplained.

Although appealing from an engineering perspective, the analyses based on linear thermoelasticity do not address the action of defects and dislocations created by microscopic yield phenomena below the CRSS and ones grown in at the solidification front. All the authors cited above assume that no defects exist at the melt/crystal interface and that the stresses on this surface are zero. Constitutive equations incorporating models for plastic deformation in the crystal due to dislocation motion have been proposed by several authors (Haasen, 1967; Alexander and Haasen, 1968; Myshlyaev et al., 1969) and have been used to describe dislocation motion in the initial stages of plastic deformation in CZ silicon crystals (Suezawa et al. 1979; Schroter et al., 1983; Lambropoulos, 1987), and silicon sheet growth (Lambropoulos et al., 1983; Dillon et al. 1987).

An interesting feature of the model proposed by Haasen (1967) is the explicit appearance of the dislocation density as a function of the stress level in the crystal. Then the dislocations grown into the crystal upon solidification are translated with the pulling rate of the crystal and multiply according to mechanisms associated with their mobility. Dillion et al. (1987) have reported temperature profiles in silicon sheets where explosive growth of the dislocation density is predicted by this model.

The understanding of the effects of dopants on dislocation mobility is minimal, although experimental evidence exists that some solutes, such as O_2 in Si (Sumino et al., 1980) and In in GaAs (Guruswamy et al., 1987), inhibit dislocation mobility. The elastoplastic constitutive equations model this effect only to the extent that the parameters are known as a function of dopant level.

Little is known about the interactions between transport properties in the melt and the production of defects at the melt/crystal interface. An exception is the swirl microdefect seen during processing of dislocation-free silicon wafers (Ravi, 1981). The origins of this defect have been shown (Chikawa and Shirai, 1977) to be related to temperature oscillations and remelting of the interface. Kuroda and Kozuka (1983) have studied the dependence of temperature oscillations on operating parameters in a CZ system, but have not linked the oscillations to convective instabilities in the melt.

The Vertical Bridgman-Stockbarger System: A Case Study of a Confined Growth System

The vertical Bridgman growth system has been the subject of the most detailed theoretical analyses and of careful experiments because the confined growth environment and the proximity of the ampoule to the furnace make it the easiest system for precise control of the thermal field. Also, for low Prandtl number fluids and small scale (ampoule diameters of approximately 1 cm) the heat transfer in the melt is dominated by conduction, so that thermal analysis of the furnace/ampoule/melt/crystal system is simplest. Investigations into the roles of furnace and ampoule design, the interactions of these features with convection in the melt, and solute segregation have led to

advances in these systems. Several of these developments are described below.

Analysis of heat transfer

In the vertical Bridgman-Stockbarger system shown in Figure 1a the axial temperature gradient needed to induce solidification is created by separating hot and cold zones with a diabatic zone in which radial heat flow from the ampoule to the furnace is supressed. Studies of conduction heat transfer analysis have focused on this geometry.

Chang and Wilcox (1974) were the first to compute the temperature field in an idealized Bridgman-Stockbarger system and to identify the importance of a perfect diabatic zone in establishing a nearly flat melt/crystal interface. Naumann (1983) and Jaskinski et al. (1983) used a one-dimensional analysis to define the minimum lengths of the hot and cold zones and the ampoule for which the temperature field in the melt and crystal reaches a steady state profile and the ampoule translation rate equals the macroscopic growth rate at the interface. Wang et al. (1984) showed the validity of this analysis through Peltier demarcation measurements of the microscopic growth rate in a well-characterized vertical Bridgman-Stockbarger system.

Investigators (Naumann and Lehoczhy, 1983; Jasinski et al., 1985) have pointed out the importance of the thermal conductivity of the ampoule material with respect to those of the melt and crystal in setting the shape of the melt/crystal interface, especially when a thick ampoule is used, as is required in the growth of materials that have extremely high vapor pressures (e.g., HgCdTe). Simple design criteria for picking ampoule materials and thickness are developed in these references. Besides setting the curvature of the melt/crystal interface, the choice of ampoule material strongly influences the radial temperature gradients in the melt, and the magnitude and direction of buoyancy-driven flow in the melt (Chang and Brown, 1983; Adornato and Brown, 1987a, b). This point is elaborated below.

Convection and segregation

When the melt wets the ampoule walls (this may not be the case in low gravity experiments; see Haynes, 1986) convection in the melt is driven only by density differences caused by temperature and concentration and by the solidification rate V_g. Chang and Brown (1983) first computed the flows in an idealized Bridgman system where the effects of the ampoule on heat transfer were neglected and the temperatures of the hot and cold zones were imposed directly on the melt and crystal with a perfect adiabatic zone separating the two regions. The analysis was based on the Boussinesq approximation for axisymmetric buoyancy-driven flow caused by temperature gradients and included analysis of heat transfer in the crystal and calculation of the interface shape. The analysis used a finite-element/Newton algorithm for solving the couple convection-solidification problem (Chang and Brown, 1984) that has proved adaptable to the analysis of other melt growth systems. The calculations are formidable; the combination of analyses of intense convection on several length scales (for momentum, heat, and solute trans-

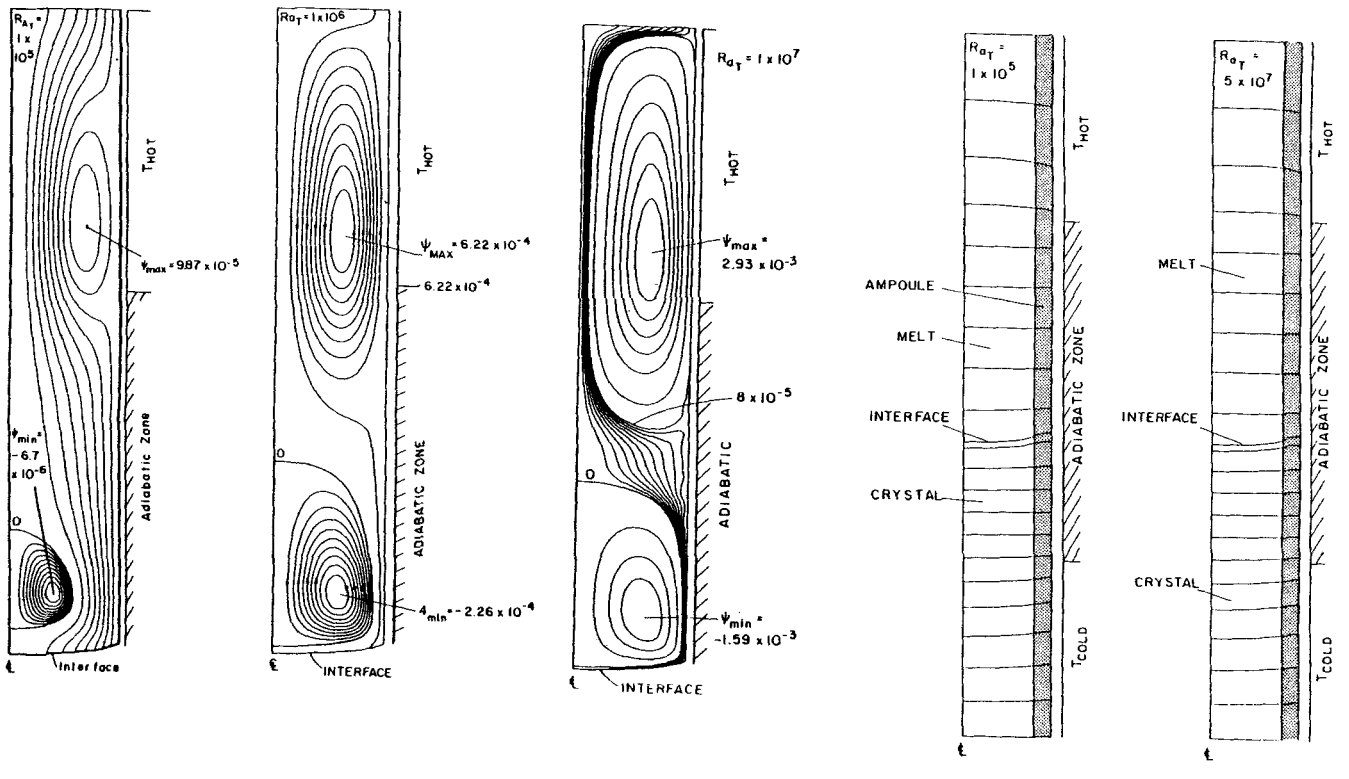

Figure 16. Sample isotherms and flow fields for growth of GaGe in vertical Bridgman system as a function of Ra_T.
From Adornato and Brown (1987b)
Streamlines are spaced at equal intervals between maximum (or minimum) for flow cells and zero

port) and the unknown interface location force the use of supercomputers for exhaustive analyses.

These results verified that heat transfer in the melt was conduction-dominated except at intense convection levels because of the low Prandtl number characteristic of semiconductor melts. The shape of the melt/crystal interface changes with convection only at these higher convection levels. The flows are cellular, with the direction and magnitude of each cell determined by the radial temperature gradients induced by the thermal boundary conditions. In the idealized system studied, the mismatch in boundary conditions at the junction of the hot zone and the adiabatic region, Figure 16, causes the temperature to increase radially and drive a flow up along the wall and down along the center of the ampoule. Secondary flows develop adjacent to the melt/crystal interface when the convection is intense enough to alter the temperature field.

Calculations of solute transport for a dilute species based on these flows were reported by Chang and Brown for a pseudo-steady-state model of directional solidification in which solute of given composition enters the ampoule at the end with melt and the crystal is pulled away at the growth rate V_g. The axial and radial segregation of solute were much more sensitive to changes in the convection level than heat transfer, because of the lower diffusivity of the species compared to heat ($Sc/Pr \gg 1$) for the melt. The results showed the transition from diffusion-controlled growth to weak convection with the associated maximum in radial segregation and finally the formation of a bulk-convection controlled boundary layer along the solidification interface, as described qualitatively by Figure 10. The impression of convection adjacent to the melt/crystal interface on radial segregation Δc was accentuated by the changes caused by the formation of the secondary flow cell adjacent to it with increasing Rayleigh number Ra_t.

Quantitative prediction of convection and solute segregation in any melt growth system requires careful control of the thermal boundary conditions that define the driving forces for the flow. Adornato and Brown (1987a,b) refined the finite-element/Newton method (1987b) and extended it to included calculation of heat transfer in the ampoule (1987a) and thermosolutal convection driven by both temperature and concentration gradients. Results are reported there for the growth of gallium-doped germanium in the Bridgman-Stockbarger furnace of Wang (1984) and the growth of silicon-germanium alloys in the constant gradient furnace designed by Rouzaud et al. (1985).

Samples of the isotherms and convection patterns computed for the Bridgman-Stockbarber system of Wang are reproduced as Figure 16. The results are shown in a frame of reference in which the melt/crystal interface is stationary and melt and crystal are translated downward at the growth rate V_g. The temperature field shows two distinct regions for the radial temperature gradients. Near the interface the temperature is highest at the center of the ampoule because of the higher thermal conductivity of the melt and the intermediate value of the conductivity of the boron nitride ampoule; the sign of the radial temperature gradient is reversed near the junction of the hot and adiabatic zones for the reason discussed above. Only the uniaxial convec-

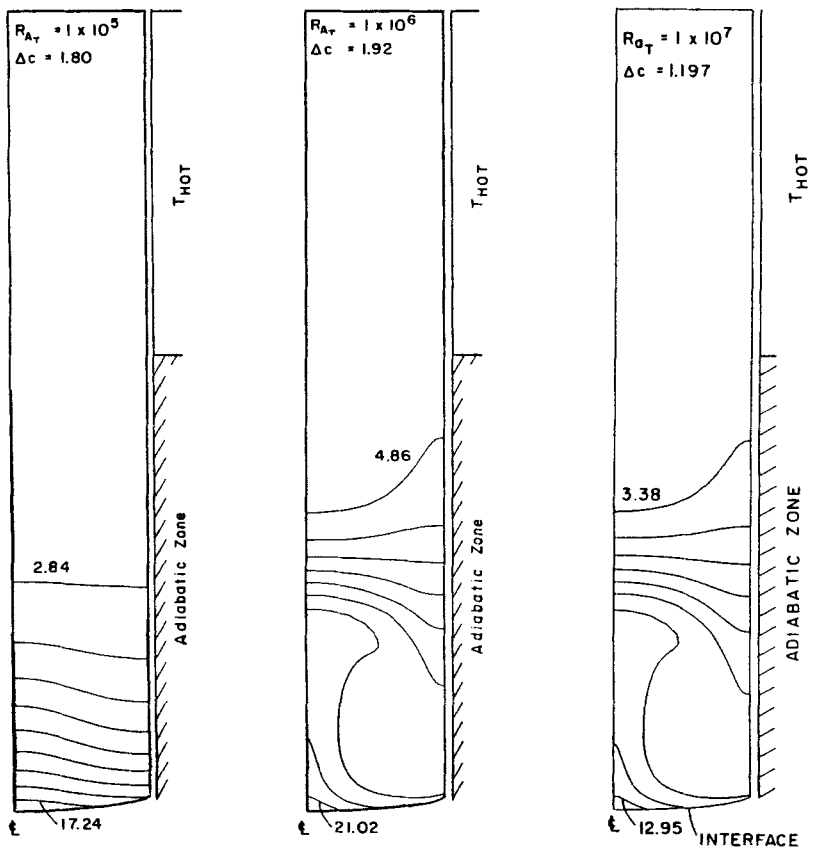

Figure 17. Solute concentration fields for growth of GaGe in the system described in Figure 16.
Growth rate V_g = 4 μm/s

tion caused by solidification is present for $Ra_t < 1 \times 10^5$; however, two toriodal flow cells driven in opposite directions by the temperature field are seen for higher values of Ra_t. The cells intensify with increasing Ra_t to the point that the streamlines corresponding to the growth velocity ($V_g = 4$ μm/s in this case) are confined to thin layers along the periphery of the cells.

Solute concentration fields are shown as Fig. 17 for the flows in Fig. 16. The diffusion-controlled profile for unidirectional solidification is unmistakable in the result for $Ra_t = 1 \times 10^5$. Radial segregation is present even without extensive bulk convection (note the intersection of isoconcentration curves with the solidification interface) because of the curvature of the melt/crystal interface. Mixing caused by the cellular flows is obvious for the higher Rayleigh numbers, and increases the radial segregation. At $Ra_t = 10 \times 10^7$ cores of constant solute composition are forming within the flow cells separated by boundary and internal layers. Calculations of the solute field for convection levels up to the value of $Ra_t = 2 \times 10^8$ appropriate for Wang's furnace are impossible with the finite element mesh used in this analysis because of under resolution of these layers.

The radial segregation predicted by these calculations is shown in Fig. 18 for three growth rates and the range of Ra_t for which computations were possible. The transitions described by Fig. 10 are apparent. Measurements of Wang (1984) for radial segregation of gallium also are shown in this figure and comparison demonstrates that convection of this system in controlled by intense laminar convection. Adornato and Brown (1987a) attempted to extrapolate the computational results for radial segregation to the Rayleigh number appropriate for the real furnace by using the power-law scaling suggested by the boundary-layer analysis described previously. The results for Δc agree to within 4–30% for the three growth rates, without any attempt to adjust the thermophysical properties of the system beyond an initial calibration of the furnace temperature profile. More importantly, the exponent for the proportionality to Pe_s ranged from 0.28 to 0.30 when the velocity scale was taken as that for a vertical buoyant boundary layer (Acrivos, 1966) so that $V_0 \sim [g\beta R^2(\Delta T)_r]^{1/2}$, where β is the coefficient of thermal expansion and $(\Delta T)_r$ is the characteristic radial temperature difference driving the flow. These values are in reasonable agreement with the simple asymptotic theory presented earlier.

Transitions to three-dimensional, time-periodic, and chaotic flows do occur in vertical Bridgman growth systems for higher convection levels with melt above solid or when the melt is below the crystal, so that the axial temperature gradient leads to an unstably stratified melt (Kim et al., 1972); see the discussion in (Brown, 1987). The implementation of an imposed axial magnetic field removes these oscillations (Kim, 1982) and reduces the motion to laminar. Several investigators have analyzed the impact of the magnetic field on solute segregation in Bridgman growth numerically (Oreper and Szekely, 1983, 1984; Kim et al., 1988) and asymptotically (Kim et al., 1988). The structure of the asymptotic analysis follows the work of Hjellming and Walker (1986), as discussed earlier.

The flows and the consequent solute segregation caused by thermosolutal convection in nondilute alloys is only beginning to be explored by experimental and computational. Recent results are discussed by Brown (1987).

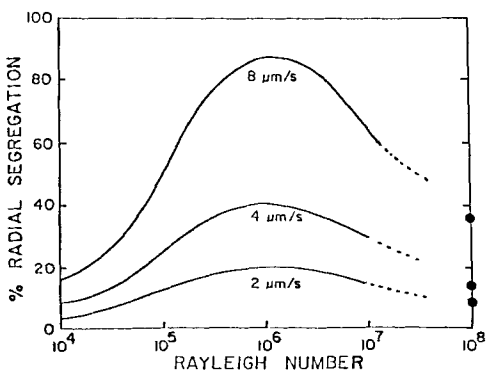

Figure 18. Radical segregation Δc as a function of Ra_t for growth of GaGe in furnace described by Figures 15 and 16.

• Results of experiments by Wang (1984)

Czochralski Crystal Growth: A Case Study of a Meniscus-Defined Growth System

The presence of the meniscus in Czochralski (CZ) growth brings new dimensions to the problems of optimization and control, as well as analysis of transport processes. Because of its relatively enormous industrial significance, CZ growth has received the most attention of any melt growth method. Also, the distinctions made using Figure 3 between different levels of modeling are most clear in the discussion of Czochralski crystal growth. The discussion here focuses on analysis of macroscopic transport processes and their influence on design and control of a CZ growth system.

Understanding of the onset of microstructured crystal growth also is very relevant to CZ systems, especially for the growth of heavily doped crystals, as in the case of adding indium to GaAs for lowering the dislocation density, discussed earlier in regard to defect formation in the crystal. Here segregation of indium into the melt during growth in a LEC system eventually leads to morphological instability, as documented by Ono et al. (1986).

Meniscus shape

Figure 6 shows a schematic representation of the inner portion of a CZ furnace formed by the melt, crystal, and crucible. The crystal is attached to the melt by the melt/ambient meniscus denoted here by ∂D_m. Neglecting traction caused by hydrodynamic forces (a good assumption for semiconductor melts with high surface tensions and low viscosities) the interface shape shown in Figure 6 as $z = f(r, \theta, t)$, is set by a balance of capillary force with gravity, by the radius and height of the crystal, by the wetting of melt on the crucible, and by the wetting condition at the melt/crystal/ambient trijunction.The hypothesis for the wetting condition at this trijunction is that a constant angle ϕ_0, shown in Figure 6, is formed between the tangents to the local melt/ambient and crystal/ambient surfaces. This angle is independent of growth rate and other macroscopic parameters. The concept of a wetting angle was first proposed by Herring (1951) for descibing crystal sintering and was adapted by Bardsley et al. (1974) for meniscus-defined crystal growth. The theoretical justification for such an angle hinges on the same arguments used to describe equilibrium contact angles formed at the trijunction of a liquid on an inert solid; see the discussion in chapter 8 of Rowlinson and Widom (1982). The use of local equilibrium in the description of this point is more restrictive in the solidification process because of the dynamic phase transfor-

mation that must be proceeding on even a molecular level near the trijunction. The implications of nonequilibrium microscopic processes and bulk hydrodynamics on this angle are not understood.

Experimental justification for specification of the angle at the point of three-phase contact comes from the results of Surek and Chalmers (1975) and others that verify that a particular value of ϕ_0 measured macroscopically can be associated with crystal growth of a material in a specific crystallographic orientation and that ϕ_0 is roughly independent of growth rate.

The second justification for the angle condition comes from the necessity of this condition for determination of the radius of the crystal at the trijunction as a function of heat transfer conditions and pull rate. This argument is simple. The dimensionless Young-Laplace equation of capillary statics gives the shape of an axisymmetric melt/ambient meniscus as

$$\frac{\partial^2 f/dr^2}{[1 + (\partial f/\partial r)^2]^{3/2}} + \frac{\partial f/\partial r}{r[1 + (\partial f/\partial r)^2]^{1/2}} = Bo[f(r, \tau) - \lambda_o] \quad (35)$$

where the radius of the crucible R_c has been taken as the length scale and $Bo \equiv \Delta\rho g R_c^2/\sigma$ is the Bond number or the square of the ratio of this scale to the capillary length $l_c \equiv (\sigma/\rho g)^{1/2}$. The lefthand side of Eq. 35 is the local mean curvature of the meniscus. The constant λ_o is a dimensionless reference value of the pressure difference across the meniscus if the curvature is zero and is determined by the constraint that the melt encloses a fixed volume. Equation 35 is a nonlinear second-order boundary-value problem, which requires two boundary conditions for solution. For a nonwetting crucible material these are

$$h(R(f, t), t) = f(R, \tau), \partial f/\partial r(1, t) = 0 \quad (36)$$

where the first condition specifies the joining of the meniscus and the crystal and the second is the wetting condition at the crucible wall. The radius of the crystal at the trijunction $R(f, \tau)$ is left undetermined and must be set by an auxillary constraint, such as the wetting angle there.

For growth of a crystal with shape $R(z, \tau)$ evolving in time the wetting angle condition is written in dimensionless form as

$$\left.\frac{\partial R}{\partial t}\right|_{z=h(R,t)} = \left[V_g(t) - \left.\frac{\partial h}{\partial t}\right|_{r=R(h,t)}\right] \tan(\phi(\tau) - \phi_0) \quad (37)$$

and describes the relationship between the rate of change of the crystal radius at the trijunction and the deviation of the local angle from the equilibrium value ϕ_0. In this expression $\phi(\tau)$ is the dynamic angle formed between the local tangents to the melt/ambient and crystal/ambient surfaces, and $V_g(\tau)$ is the dimensionless pull rate of the crystal. For steady state growth, Eq. 37 simple sets the angle with what must be a solid cylinder of constant radius. The importance of the dynamical form of Eq. 37 is brought out in the next section.

When the crucible is large enough that its wetting properties have no influence on meniscus shape, i.e., the meniscus becomes flat across the melt surface, the possible shapes come from the collection for unbounded asymmetric interfaces reported by Huh and Scriven (1969; also see Paddy, 1971). This is a good approximation for Czochralski growth of large crystals where the region of influence of surface tension σ, measured by the capillary length $l_c \equiv (\sigma/\rho g)^{1/2}$, is approximately a centimeter. Hurle (1983) developed a closed-form approximation to these meniscus shapes, described by the shape function $f(r)$, which is valid in this limit.

Heat transfer analysis: thermal-capillary models

Numerous analyses of various aspects of heat transfer in the CZ system have been reported; many of these are referenced by either Kobayashi (1981) or Derby and Brown (1986b). The analyses vary in complexity and purpose from the simple one-dimensional or "fin approximations" designed to give order-of-magnitude estimates for the axial temperature gradient in the crystal (Billig, 1956), to complex system-oriented calculations designed for optimization of heater design and power requirements (Williams and Reusser, 1983; Dupret et al., 1986). The later large-scale calculations include radiation between components of the heater and the crucible assemblies as well as conduction and convection.

The dynamics of the Czochralski system can only be described by heat transfer models that include the interaction of the shape of the meniscus—referred to as thermal-capillary models (TCM)—because only these give self-consistent determination of the meniscus shape, crystal radius, and heat transfer in each phase.

Billig (1956) realized this point and used a one-dimensional heat transfer analysis for the crystal with assumptions about the temperature field in the melt to derive the relationship.

$$R \sim V_g^2 \quad (38)$$

which has been heavily used in qualitative discussions of crystal growth dynamics. K.M. Kim et. al. (1983) presented the empirical correlation for silicon growth

$$R = A/(V_g + B) \quad (39)$$

where A and B are constants that depend on the details of the system and are determined from experiments.

Kobayashi (1981) presented the first computer simulations that consider determination of the crystal radius as part of the analysis, but avoided the capillary problem by considering a flat melt/ambient surface, which is consistent with taking $\phi_0 = 90°$. Calculations were performed for a fixed crystal radius and then the growth rate was adjusted to balance the heat flux into the crystal. Crowley (1983) was the first to present numerical calculations of a conduction-dominated heat transfer model for simultaneous determination of the temperature fields in crystal and melt, and the shapes of the melt/crystal and melt/ambient surfaces for an idealized system with a melt pool so large that no interactions with the crucible are considered. She used a time-dependent formulation of the thermal-capillary model and computed the shape of an evolving crystal from a short initial configuration.

In a series of papers Derby and Brown (1986a, b, c, 1987, 1988) developed a detailed TCM that includes calculation of the temperature field in the melt, crystal, and crucible, the location of the melt/crystal and melt/ambient surfaces, and the crystal shape. The analysis is based on a finite-element/Newton method that is described in detail by Derby and Brown (1987). The heat transfer model included conduction in each of the

phases and an idealized model for radiation from the crystal, melt, and crucible surfaces without systematic calculation of view factors and diffuse-gray radiative exchange.

Results from a quasisteady-state model (QSSM) valid for long crystals and a constant melt level (assuming some form of automatic replenishment of melt to the crucible) verified the correlation in Eq. 39 for the dependence of radius on growth rate (Derby and Brown, 1986a) and predicted changes in the radius, the shape of the melt/crystal interface (a measure of radial temperature gradients in the crystal), and the axial temperature field with important control parameters such as the heater temperature and the level of melt in the crucible. Processing strategies for holding the radius and interface shape constant as the melt volume decreases through a typical batchwise growth cycle are presented by Derby and Brown (1986b), as computed by a strategy for augmenting the Newton method with the additional constraints for each control parameter.

Sristava et al. (1985; Ramachandran and Dudokovic, 1985) extended the analysis of a QSSM to include diffuse-gray radiation by computing view factors by approximating the shapes of the crystal and melt by a few standard geometrical elements and incorporating analytical approximations to the view factors. Atherton et al. (1987) developed a scheme for self-consistent calculation of view factors and radiative fluxes within the finite-element framework and implemented this in the QSSM. Several of the results from this work are described here.

Figure 19 shows sample isotherms and interface shapes predicted by the QSSM for calculations with decreasing melt volume in the crucible, as occurs in the batchwise process. Because the crystal pull rate and the heater temperature are maintained at constant values for this sequence, the crystal radius varies with the varying heat transfer in the system. Two effects are noticeable. First, decreasing the volume exposes the hot crucible wall to the crystal, thereby heating it and causing the decreasing radius seen for dimensionless melt volumes V_m of 3.1 and 2.3. Second, heat transfer from the crucible to the melt becomes ineffective for low volumes, causing a decrease in the temperature of the melt and an increase in the crystal radius. For the lowest volume, the melt temperature at the bottom of the crucible drops below the melting point and a lump of solid forms at the center; the growth is terminated in the simulation by the merging of this mass of solid with the melt/crystal interface. Either insulating or inputting heat along the bottom leads to a monotonic decrease in the radius to much lower melt volumes, with an almost linear relationship ($R \sim V_m$) when the bottom is heated.

The results of the thermal-capillary models discussed so far have all neglected the influence of convection in the melt in transporting heat to the solidification interface. The status of convection calculations that neglect the coupling to global heat transfer and capillary consideration is discussed following the next section. The union of thermal-capillary analysis with detailed convection calculations is also discussed in the subsection on melt flow.

Process stability and control

Operationally, automatic control of the crystal radius by varying either the input power to the heater or the crystal pull rate has been necessary for the reproducible growth of crystals with constant radius. Techniques for automatic diameter control have been utilized since the establishment of Czochralski growth with either optical imaging of the crystal or direct mea-

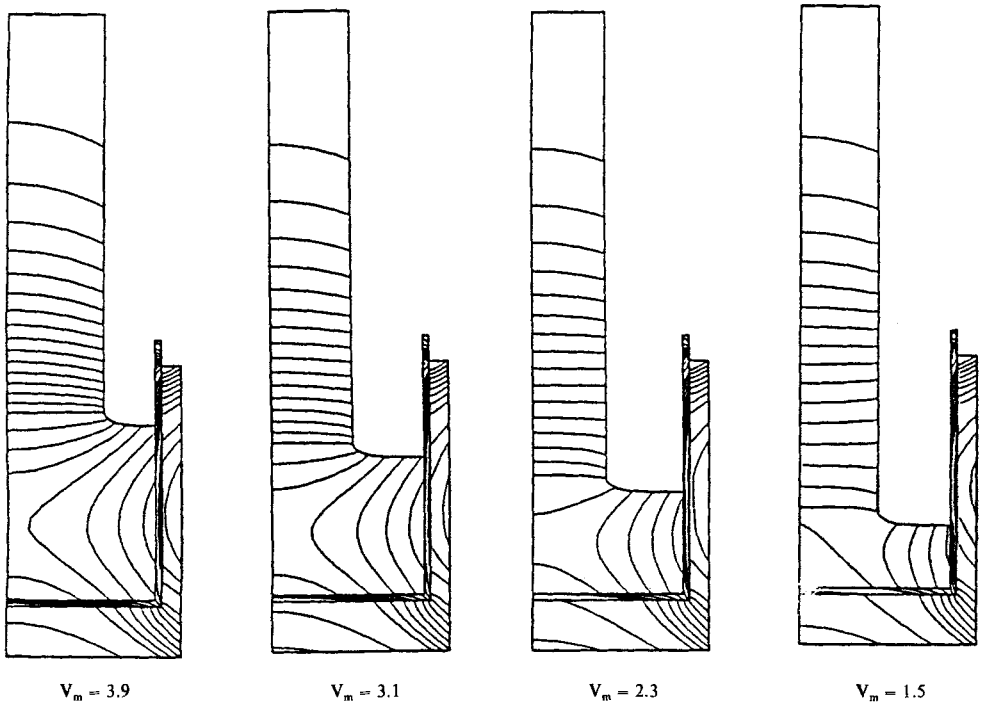

Figure 19. Sample isotherms and interface shapes computed for the QSSM for CZ crystal growth (Atherton et al., 1987).

Model includes detailed radiation between surfaces of melt, crystal, and crucible
Isotherms spaced at 10 K increments in melt and at 30 K increments in other phases

surement of the crystal weight used to determine the instantaneous radius. Hurle (1977) reviews the techniques currently used for sensing the radius. Bardsley et al. (1977a, b) describe control based on measurement of the crystal weight.

The details of the control strategy have received much less attention. The theoretical (Steel and Hill, 1975) and experimental (Hurle et al., 1986) analyses of the transfer function for CZ growth are notable exceptions. Algorithms for model-based control are just being developed and are discussed below.

The implementation of a control algorithm using any sensing technology depends on the dominant dynamics of the Czochralski process, especially the stability of the process to perturbations in the thermal field and the interface shapes and the batchwise transient introduced by the decreasing melt volume. The control strategies differ substantially according to whether the process is stable or inherently unstable. This issue is discussed here in terms of the several notions for stability introduced by Hurle (1985) that are relevant to meniscus-defined crystal growth. Three types of instabilities are distinguished according to the time scales for the disturbances; these are capillary instabilities of the meniscus, dynamic instability of the entire thermal-capillary system, and convective instabilities of the melt. The first two mechanisms are discussed below. Convective instabilities are considered in the next section.

First, the meniscus shape may become unstable in the sense that small perturbations to it cause the melt to separate from the crystal on the time scale of a capillary-induced motion of the surface. This time scale is proportional to the capillary wave speed, which is a few seconds for the thermophysical properties of molten silicon. The capillary stability of menisci shapes important in CZ growth is analyzed by several authors (Mika and Uelhoff, 1975; Boucher and Kent, 1977) using arguments from energy stability theory for equilibrium configurations. Meniscus shapes that are stable to capillary instabilities are feasible for a range of contact angles and interface heights.

Surek (1976; Surek et al., 1980) introduces the notion of "dynamic stability" for meniscus-defined crystal growth systems. He considers the question of whether a meniscus-defined growth system subjected to a perturbation to the crystal shape at fixed pull rate will return to the initial shape or diverge unstably away from it. The concept of dynamic stability does not consider the effect of the batchwise drop in the melt volume on the evolution of the perturbation, even though the time scale for the decreasing melt volume and for the growth of the crystal are essentially the same except when the crucible is much larger in diameter than the crystal being grown.

The initial analysis of Surek (1976) considers the influence of the wetting condition at the trijunction, Eq. (37) and the Young-Laplace equation for meniscus shape, but neglects the influence of heat transfer on the dynamics of the system. Without heat transport the location of the melting point isotherm is unspecified, so the dynamics of the height of the trijunction $h(f, \tau)$ is unknown. On the basis of an isothermal analysis, Surek shows that the floating zone techniques and die-defined methods for growth of thin solid sheets are stable to perturbations in the meniscus height, but that the CZ method is inherently unstable. Refinements to the analysis that include simple descriptions of the interactions between heat transfer and the meniscus height show that conditions exist for stable operation (Tatarchenko and Brenner, 1980; Surek et al., 1980) without considering batchwise transients.

Integration of a time-dependent thermal-capillary model for CZ growth (Derby and Brown, 1987; Derby et al., 1988) also has illuminated the idea of dynamic stability. Derby and Brown (1987) first constructed a time-dependent TCM that included the transients associated with conduction in each phase, the evolution of the crystal shape in time, and the decreasing of the melt level caused by conservation of volume, but idealized radiation to a uniform ambient. The technique for implicit numerical integration of the transient model was built around the finite-element/Newton method used for the QSSM. Linear and nonlinear stability calculations for the solutions of the QSSM (neglecting the batchwise transient) showed the CZ method to be dynamically stable; small perturbations in the system at fixed operating parameters decayed in time and changes in the parameters caused evolution of the process to the expected new solutions of the QSSM. The stability of the CZ process has been at least partially verified experimentally by the uncontrolled, stable growth of small-diameter germanium (Robertson and Young, 1975) and silicon crystals (M. Wargo, private communication, Massachusetts Institute of Technology).

Atherton et al. (1987; also see Derby et al., 1988) have expanded the calculations with the dynamic model to include diffuse-gray radiation between components of the enclosure and have reached essentially the same conclusions regarding the stability of the process. However, they discovered a new mechanism for damped oscillation of the crystal radius caused by the radiative interaction between the crystal surface just above the melt level and the hot crucible wall. These oscillations are especially apparent when the vertical temperature gradient in the crystal is low, so that radiative heat transport has a dominating influence.

The dynamic stability of the quasisteady-state process suggests that active control of the CZ system only has to account for random disturbances to the system about its set point and for the batchwise transient caused by the decreasing melt volume. Derby and Brown (1987) implemented a simple proportional-integral (PI) controller that coupled the crystal radius to a set point temperature for the heater in an effort to control the dynamic CZ model with idealized radiation. Figure 20 shows the shapes of the crystal and melt predicted without control, with purely integral control, and with PI control. The oscillations in the radius about the set point predicted with integral control are not unexpected. Oscillations in control of systems governed by linear models (Stephanopoulos, 1984) and the occurrence of Hopf bifurcations in nonlinear models (Chang and Chen, 1984) have both been predicted with integral control. Indeed, the oscillations shown for PI control are anticipated from the appearance of a Hopf bifurcation in the QSSM with increasing gain of the integral part of the controller (Derby and Brown, 1987). Simple PI control removes the oscillations and leads to a constant radius throughout a large portion of the growth run. Atherton et al. (1987) have extended these calculations to included diffuse-gray radiation and have shown that PI control of the crystal radius is much more difficult there because the increasing influence of radiation at the melt level drops causes a single set of gain values to be inappropriate for the whole growth run.

It remains to be shown that the dynamics predicted by thermal-capillary models adequately represents a real CZ system. A first step in this direction has been taken by Thomas et al. (1988) by a direct comparison between predictions of a dynamic

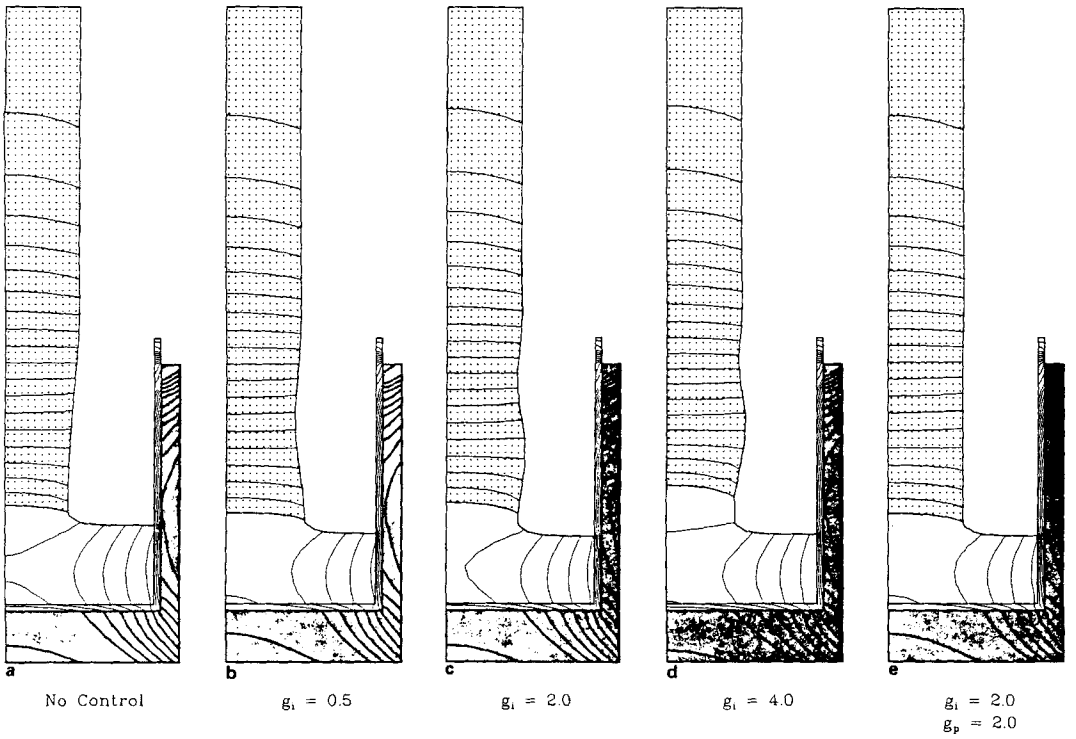

Figure 20. Isotherms and interface shapes for time τ = 1.0 for batchwise simulations of CZ growth.
Results shown for uncontrolled, integral control, and PI control simulations; isotherms spaced as in Figure 19. The integral (g_i) and proportional (g_p) gains for each simulation are listed.
From Atherton et al. (1987)

TCM for liquid-encapsulated CZ growth of GaAs to the response of an experimental system using a large (2 kGauss) axial magnetic field. The pull rate and heater temperature in the calculation are varied with time according to prescribed histories taken from experimental data. The shape of the crystal and the temperature field predicted by the simulation are shown in Figure 21 as a function of time during the batch process. The shape of the crystal agrees qualitatively with that produced in the experiment. The quantitative value of the radius at any time is within 30% of the experimental value; this difference is well within the error caused by uncertainties in the experiment and by poor knowledge of thermophysical property data used in the model.

Convection and segregation

Melt Flow. Although analysis of convection and segregation in Czochralski growth has received the most attention of any melt growth system, the large size of a typical puller and the presence of a meniscus make the simulations the most difficult of any system. The real flows in large-scale systems are most probably three-dimensional and temporally chaotic; detailed analysis of such motions stretches the limits of even the largest calculations performed today.

Axisymmetric flow calculations that neglect the determination of the shapes of the melt/crystal and melt/ambient phase boundaries have been carried out by a number of investigators for some time. The results before 1985 are reviewed by Langlois (1985) and focus on the interactions of flows driven by crucible and crystal rotation, buoyancy, and surface-tension gradients. Starting with the initial calculations of Kobayashi (1978), most of these analyses have focused on predicting the multicellular structure of the flows caused by combinations of various driving forces.

More recent simulations concentrate on the onset of time-periodic convection, which marks the onset of a dominant mechanism for dopant striations in the crystal and on the effect of an imposed magnetic field on this transition. Crochet et al. (1983) first computed the onset of an axisymmetric time-periodic motion in CZ flow driven by heating of the sidewall. The flow is caused by the competition between flow cells created by an instability that leads to separation of the hydrodynamic boundary layer along the crucible sidewall. Accurate calcula-

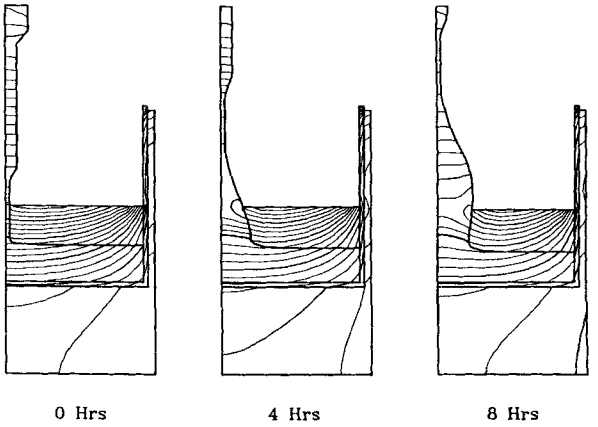

Figure 21. Isotherms and interface shapes for selected times during batchwise simulations of GaAs crystal in LEC growth.
From Thomas et al. (1988)

tions must resolve this boundary layer. A simulation reported by Crochet et al. is represented by the plot in Figure 22 of the kinetic energy in the flow as a function of time for $Gr \equiv g\beta(T_{wall} - T_m)R_c^3/\nu^2 = 1 \times 10^7$, where T_{wall} is the constant temperature of the crucible wall. The oscillations develop from some initial state and tend toward constant values of the amplitude and frequency. The flow patterns and temperature fields reported by Crochet et al. for several different times in this simulation are shown in Figure 23. The interaction between the two largest torodial vortices is apparent.

Patera and Tangborn (see Tangborn, 1987) has reproduced the oscillations seen by Crochet et al. using a spectral-element simulation with flat phase boundaries. They demonstrated that underresolution of the boundary layer leads to spurious oscillations at lower Grashof numbers. Others have computed unsteady convection in a similar model for axisymmetric convection in CZ bulk flow.

Langlois (1982, 1984) first demonstrated numerically the experimentally seen damping of convection caused by an imposed axial magnetic field on unsteady convection and the possibility of achieving steady, axisymmetric flows. Mihelcic and Winegrath (1985) and Tangborn (1987) have presented similar results with more emphasis on the transition between steady and oscillatory flow caused by increasing the magnetic field strength. Increasing the field beyond the level necessary to stabilize the flow causes decreased mixing in the melt and leads to radial nonuniformity of dopants in the crystal, as would be the case for weak convective mixing indicated by Figure 10. Opreper and Szekely (1983) documented this effect and Hjellming and Walker (1986) presented asymptotic analysis for the flow and temperature fields in this limit.

Numerical simulations that combine the details of the thermal-capillary models described previously with the calculation of convection in the melt should have the capability of giving predictive analysis of the heat transfer in the CZ system. Sackinger et al. (1988b) have added the calculation of steady-state, axisymmetric convection in the melt to the thermal-capillary model for quasisteady-state growth of a long cylindrical crystal. The calculations include melt motion driven by buoyancy, surface-tension, and crucible and crystal rotation. Figure 24 shows sample calculations for growth of a 3 in. (7.6 cm) dia. silicon crystal as a function of the depth of the melt in the crucible.

The radial temperature difference imposed by the heater arrangement drives a large torodial flow cell that moves up the wall and down toward the center of the crucible. For the deepest

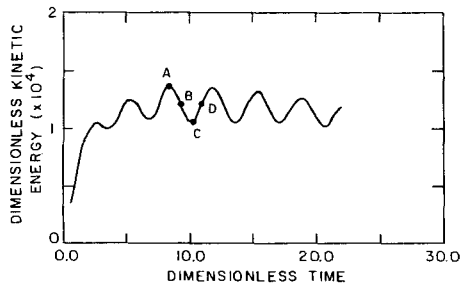

Figure 22. Kinetic energy as a function of time in simulation of CZ bulk flow for Grashof number $Gr = 1 \times 10^7$.

From Crotchet et al. (1983)

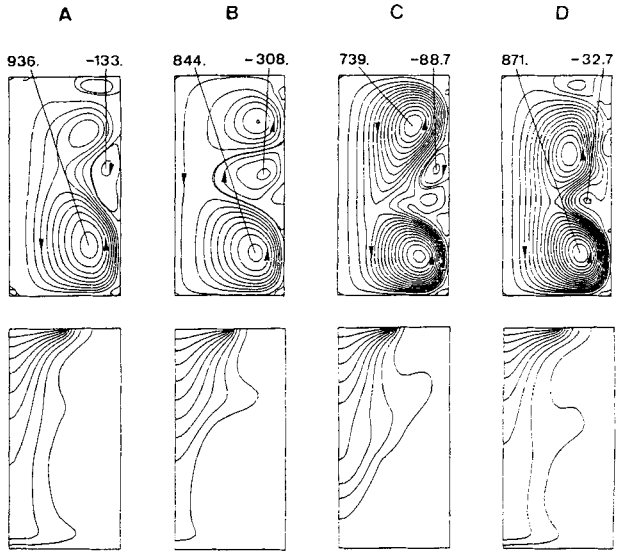

Figure 23. Streamlines and isotherms for selected times during simulation shown in Figure 22.

melt volumes the flow is separated along the wall. This steady axisymmetric motion is probably not stable. Time-periodic oscillations caused by the instability of this separation have been reported at values of the Grashof number below the values that correspond to the calculations in Figure 24. Adding an axial magnetic field leads to reattachment of the flow cell to the wall of the crucible and to the flow structure predicted by Hjellming and Walker (1986) at high field levels.

The flow separation along the crucible sidewall disappears and separation along the bottom appears as the melt level is lowered; this is shown in Figure 24. The melt/crystal interface deforms to be convex at the center of the crystal as it senses the cold crucible bottom with the decreasing melt depth. This interface flipping is well documented in experimental systems and is also seen in calculations based solely on conduction in the melt.

Few calculations of three-dimensional convection in CZ melts (or other systems) have been presented because of the prohibi-

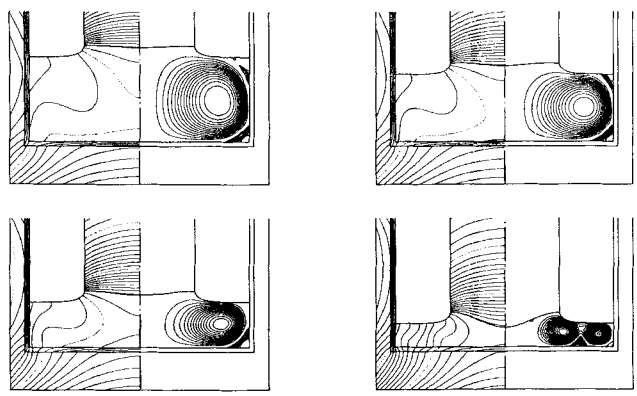

Figure 24. Streamlines and isotherms for growth of Si in a prototype CZ system.

Results with self-consistent calculation of interface and crystal shapes using QSS TCM and the condition that the crystal radius remain constant

Calculations are for decreasing melt volume; Grashof number Gr (scaled with maximum temperature difference in melt) varies between 1.0×10^7 and 2.0×10^7 with decreasing melt volume

tive expense of such simulations. Mihelcic et al. (1984) have computed the effect of asymmetries in the heater temperature on the flow pattern and show that crystal rotation will eliminate three-dimensional convection driven by this mechanism. Recently, Tangborn and Patera (Tangborn, 1987) have used a spectral-element method combined with linear stability analysis to compute the stability of axisymmetric flows to three-dimensional instabilities. Such a stability calculation is the most essential part of a three-dimensional analysis, since nonaxisymmetric flows are undesirable.

Solute Transport. Burton et al. (1953b) originated the boundary layer analyses for solute transport in CZ crystal growth described earlier, which has been the starting point for studying axial solute segregation in CZ growth. Wilson (1980b) has refined this analysis by including full numerical calculation of the self-similar velocity field due to crystal rotation instead of using the asymptotic approximation of Cochran (1934). Wilson (1980a, b) also uses the transient, self-similar velocity field caused by crystal rotation to analyze the time-dependent axial dopant striations caused by a fluctuating local growth rate. By simultaneous calculation of the flow and the solute field without (1980a) and with (1980b) accounting for the possible backmelting of the solid, she demonstrates periodic axial striations in the concentration field that are extremely similar to ones reported in CZ growth for systems with poor thermal symmetry that resulted in growth rate fluctuations proportional to the crystal rotation rate (Carruthers and Witt, 1975). Earlier, Hurle et al. (1968) made the connection between dopant striations and temperature oscillations using a simpler model.

Analysis of solute transport in the presence of a magnetic field has received considerable attention. Hurle and Series (1985) (also see Cartwright et al., 1987) use the self-similar form of the velocity field near a rotating crystal as a framework for examining the role of an axial magnetic field in modifying axial segregation in the crystal.

Lee et al. (1984) reported the only detailed calculations of solute transport in Czochralski growth for oxygen transport in the presence of an axially aligned magnetic field. Their results indicated that oxygen transport is slowed by the damping of convection and that the structure of the flow cells has a significant effect on the transfer rate, if the flow is steady. Hoshikawa et al. (1980) first demonstrated the control of oxygen concentration in CZ-grown silicon using an applied magnetic field; also see Kim and Smetana (1986). More recent analysis by Kim and Langlois (1986) of boron transport in CZ growth with an axial magnetic field shows large radial variations in boron concentration when bulk convection is weak. Such large variations have been reported in several unpublished experimental studies. Hjellming and Walker (1987) have presented an asymptotic analysis valid for solute transport controlled by convection caused by crystal growth.

Summary and Outlook

Pioneering efforts in the understanding of transport processes in melt crystal growth have elucidated the fundamental mechanisms important in these systems and are the beginning of comprehensive understanding of property/processing relationships for electronic materials. The segregation analysis of Burton, Prim, and Slichter, the analysis of the onset of morphological instabilities by Mullins and Sekerka, and the documentation of the transitions to chaotic convection in melt crystal growth by Witt and his collaborators are examples of such seminal investigations.

Each of these efforts has spawned nearly a generation of scientific exploration and engineering application of these concepts. As this paper indicates, the level of generic understanding of transport processes and macroscopic properties of the crystal is good. Even so, quantitative prediction of the performance of specific crystal growth systems and the design and optimization of these systems based solely on theoretical understanding is not yet feasible. The design of systems for specific materials still involves a great deal of experimental input and empiricism. The reasons for this limitation are many.

First, the role of system design in the details of convection and solute segregation in industrial-scale crystal growth systems has not been adequately studied. This deficiency is mostly due to the fact that numerical simulations of the three-dimensional, weakly turbulent convection present in these systems are at the very limit of what is computationally feasible today. New developments in computational power may lift this limitation. Also, the extensive use of applied magnetic fields to control the intensity of the convection makes the calculations much more feasible.

Even if the extensive calculations needed to parameterize the dependence of segregation and heat transfer on operating conditions can be performed, they may not be justified in the sense that the results cannot be supported either by the level of quantitative characterization of a typical crystal growth system or by the accuracy of the data base for the thermophysical properties of exotic semiconductor alloys, especially under high-temperature processing conditions. The first deficiency requires extensive developments in the technology of sensors for monitoring variables during the crystal growth process—e.g., the temperature gradients in the crystal, which are directly responsible for defect generation in the solid. It is becoming clear that characterization of the thermophysical properties of these materials is a prerequisite for accurate understanding of the processing conditions for any melt crystal growth system.

The most conspicuous shortcomings of modern theory of crystal growth appear when the links between macroscopic processing conditions and the formation of crystalline defects are considered. Other than the intuition derived by applying linear thermoelasticity theory to the calculation of stress fields in the cooling solids, no guidelines exist for designing growth systems. Elucidating the mechanisms of defect formation and the importance of the chemistry of the melt and hence transport processes in these mechanisms are important frontiers in materials processing of electronic materials.

Acknowledgment

The writing of this paper and the research contributions of the crystal growth group at the Massachusetts Institute of Technology described within it were made possible by grants from the Microgravity Sciences Program of the National Aeronautics and Space Administration, the Defense Advanced Research Project Agency, and the Mobil Foundation and by a Teacher-Scholar Award from the Camille and Henry Dreyfus Foundation to the author. The author is deeply indebted to these sponsors. The author is also grateful to the many colleagues who have contributed to this paper through their research and discussions with the author; these include L. J. Atherton, S. R. Coriell, J. J. Derby, D.-H. Kim, G. B. McFadden, P. H. Sackinger, P. D. Thomas, C. A. Wang, M. J. Wargo, and A. F. Witt. The author is especially grateful to E. D. Bourret for her critical reading of this manuscript.

Notation

$\boldsymbol{B}$ = magnetic field
B_o = magnitude of magnetic field
$c(\boldsymbol{x}, Dt)$ = dimensionless concentration field
c_o = far field level of concentration
c^* = characteristic concentration scale
D = molecular diffusivity of solute in melt
$\boldsymbol{e}_g$ = unit vector in direction of gravity
$f(r)$ = dimensionless meniscus shape function
$\boldsymbol{F}_b(\boldsymbol{x})$ = dimensionless applied body force field
$\boldsymbol{F}_s(\boldsymbol{x})$ = dimensionless surface force
g = acceleration of gravity
G = dimensionless axial temperature gradient
$h(r)$ = dimensionless melt/crystal interface shape function
H = dimensionless mean curvature of interface
k = equilibrium partition coefficient, Eq. 1
k_{eff} = effective segregation coefficient
k_i = thermal conductivity of phase i
l_c = capillary length, $(\sigma/\rho_m g)^{1/2}$
L^*, L = characteristic length scale
m = dimensionless slope of liquids curve
$\boldsymbol{n}$ = unit normal vector to melt/ambient meniscus
$\boldsymbol{N}$ = unit normal vector to melt/crystal interface
$p(\boldsymbol{x}, t)$ = dimensionless pressure field
r = dimensionless radial coordinate
R = dimensionless crystal radius
t = dimensionless time
$\boldsymbol{t}$ = unit tangent vector to melt/ambient meniscus
$\boldsymbol{T}$ = unit tangent vector to melt/crystal interface
$T(\boldsymbol{x}, t)$ = dimensionless temperature field
T_m = melting temperature
T^* = characteristic temperature scale
$\boldsymbol{v}(\boldsymbol{x}, t)$ = dimensionless velocity field
V_g = growth rate
V_o = velocity scale for bulk motion
V^* = characteristic velocity scale
$\boldsymbol{V}_s(\boldsymbol{x}, t)$ = dimensionless velocity of solid surfaces
$\boldsymbol{x}$ = vector of dimensionless coordinates

Greek letters

α_i = thermal diffusivity of phase i
β_c = coefficient of solutal expansion
β_t = coefficient of thermal expansion
γ = melt/crystal interfacial energy
$\tilde{\Gamma}$ = melt/crystal capillary length, $\gamma/\Delta H_f$
δ = dimensionless stagnant film thickness
Δ = dimensionless boundary layer thickness
ΔH_f = latent heat of fusion
Δc^* = characteristic scale for concentration difference
$\Delta\rho$ = density difference between melt and ambient
ΔT = maximum temperature difference
ΔT^* = characteristic temperature difference
ν = momentum diffusivity, μ/ρ_m
μ = Newtonian viscosity of melt
Ω = characteristic rotation rate
ρ_i = mass density of phase i
σ = interfacial tension of melt/ambient meniscus
σ^* = characteristic value of σ
τ = deviatoric stress tensor
∂D_b = boundary of computational domain
∂D_{bl} = fraction of boundary adjoining solid surfaces

Subscripts

m = melt phase
s = solid of crystal phase
I = melt/crystal interface
o = reference values

Superscripts

$\sim$ = dimensional value of parameter

Literature Cited

Abernathy, J. R., and F. Rosenberger, "Time-Dependent Convective Instabilities in a Closed Vertical Cylinder Heated from Below," *J. Fluid Mech.*, **160,** 137 (1985).

Acrivos, A., "On the Combined Effect of Forced and Free Convection Heat Transfer in Laminar Boundary Layer Flows," *Chem. Eng. Sci.*, **21,** 343 (1966).

Adornato, P. M., and R. A. Brown, "The Effect of Ampoule on Convection and Segregation During Vertical Bridgman Growth of Dilute and Nondilute Binary Alloys," *J. Crystal Growth,* **80,** 155 (1987a).

———, "Petrov-Galerkin Methods for Natural Convection in Directional Solidification of Binary Alloys," *Int. J. Num. Meth. Fluids,* **7,** 57 (1987b).

Atherton, L. J., J. J. Derby, and R. A. Brown, "Radiative Heat Exchange in Czochralski Crystal Growth," *J. Crystal Growth,* **84,** 57 (1987).

Alexander, H., and P. Haasen, "Dislocations and Plastic Flow in the Diamond Structure," *Solid State Phys.*, **22,** 28 (1968).

Bardsley, W., F. C. Frank, G. W. Green, and D. T. J. Hurle, "The Weighing Method of Automatic Czochralski Crystal Growth. I: Basic Theory," *J. Crystal Growth,* **23,** 341 (1977a).

Bardsley, W., D. T. J. Hurle, and G. C. Joyce, "The Weighing Method of Automatic Czochralski Crystal Growth. II: Control Equipment," *J. Crystal Growth,* **40,** 13 (1977b).

Bennett, M. J., R. A. Brown, and L. H. Ungar, "Nonlinear Interactions of Interface Structures of Differing Wavelength in Directional Solidification," *Proc. 1986 Int. Symp. Physics of Structure Formation,* Springer, Berlin (1988).

Billig, E., "Growth of Monocrystals of Germanium from an Undercooled Melt," *Proc. Roy. Soc. (Lond.),* **A235,** 37 (1956).

Boucher, E. A., and H. J. Kent, "Capillary Phenomena. III: Properties of Rotationally Symmetric Fluid Body with One Asymptote—Holms," *Proc. Roy. Soc. (Lond.),* **A356,** 61 (1977).

Bourret, E. D., J. J. Derby, and R. A. Brown, "One-dimensional Modeling of Transients in Directional Solidification of Nondilute Binary Alloys," *J. Crystal Growth,* **71,** 587 (1985).

Brice, J. C., *The Growth of Crystals from Liquids;* North-Holland, New York, (1976).

Burton, J. A., R. C. Prim, and W. P. Slichter, "The Distribution of Solute in Crystals Grown from the Melt. I. Theoretical," *J. Chem. Phys.*, **21,** 1987 (1953a).

Burton, J. A., J. A. Kolb, W. P. Slichter, and J. D. Struthers, "The Distribution of Solute in Crystals Grown from the Melt. II: Experimental," *J. Chem. Phys.*, **21,** 1991 (1953b).

Brown, R. A., "Convection and Species Transport," *Materials Sciences in Space,* B. Feuerbacher, H. Hamacher, R. J. Naumann, eds., Springer, Berlin, 55 (1986).

———, "Convection and Solidification in Melt Crystal Growth," *Advanced Crystal Growth,* P. Dryburgh, ed., Prentice Hall, New York, 41 (1987a).

Brown, R. A., N. Ramprasad, and M. J. Bennett, "Numerical Analysis of Solidification Microstructure," *Supercomputer Research in Chemistry and Chemical Engineering,* D. G. Truhlar, K. Jensen, eds., Am. Chem. Soc. Symp. Ser., Washington, DC (1987).

Camel, D., and J. J. Favier, "Scaling Analysis of Convective Solute Transport and Segregation in Bridgman Crystal Growth from the Doped Melt," *J. Physique,* **47,** 1001 (1986).

Carlberg, T., T. B. King, and A. F. Witt, "Dynamic Oxygen Equilibrium in Silicon Melts During Crystal Growth by the Czochralski Technique," *J. Electrochem. Soc.*, **129,** 189 (1982).

Carpenter, B., and G. M. Homsy, "The Effect of Surface Contamination on Thermocapillary Flow in a Two-Dimensional Slot. 2: Partially Contaminated Interfaces," *J. Fluid Mech.*, **155,** 429 (1985).

Carruthers, J. R., "Origins of Convective Temperature Oscillations in Crystal Growth Melts," *J. Crystal Growth,* **32,** 13 (1976).

———, "Thermal Convection Instabilities Relevant to Crystal Growth from Liquids," *Preparation and Properties of Solid State Materials,* **3,** W. R. Wilcox, R. A. Lefever, eds., Dekker (1977).

Carruthers, J. R., and A. F. Witt, "Transient Segregation Effects in Czochralski Growth," *Crystal Growth and Characterization;* R. Ueda, J. B. Mullins, eds., North-Holland, Amsterdam (1975).

Cartwright, R. A., N. El-Kaddah, and J. Szekely, "The Effect of an Axial Magnetic Field at the Interface of a Crystal Grown by the Czochralski Method," *IMA J. Appl. Math.*, **35,** 175 (1985).

Cartwright, R. A., D. T. J. Hurle, R. W. Series, and J. Szekely, "The Influence of Crucible Rotation on the Effective Distribution Coefficient in Czochralski and Magnetic Czochralski Growth," *J. Crystal Growth*, **82**, 327 (1987).

Chang, C. E., and W. R. Wilcox, "Control of Interface Shape in Vertical Bridgman-Stockbarger Technique," *J. Crystal Growth*, **21**, 135 (1974).

Chang, C. J., and R. A. Brown, "Radial Segregation Induced by Natural Convection and Melt/Solid Interface Shape in Vertical Bridgman Growth," *J. Crystal Growth*, **63**, 343 (1983).

———, "Natural Convection in Steady Solidification: Finite-Element Analysis of a Two-phase Rayleigh-Benard Problem," *J. Comput. Phys.*, **53**, 1 (1984).

Chang, H., and L. Chen, "Bifurcation Characteristics of Nonlinear Systems Under Conventional PID Control," *Chem. Eng. Sci.*, **39**, 1127 (1984).

Chikawa, J., and S. Shirai, "Melting of Silicon Crystals and a Possible Origin of Swirl Defects," *J. Crystal Growth*, **39**, 328 (1977).

Ciszek, T. F., "Techniques for the Crystal Growth of Silicon Ingots and Ribbons," *J. Crystal Growth*, **66**, 655 (1984).

Cochran, W. G., "The Flow Due to Rotating Disk," *Proc. Camb. Phil. Soc.*, **30**, 365 (1934).

Coriell, S. R., and R. F. Sekerka, "Lateral Solute Segregation During Unidirectional Solidification of a Binary Alloy with a Curved Solid-Liquid Interface," *J. Crystal Growth*, **46**, 470 (1979).

Coriell, S. R., M. R. Cordes, W. J. Boettinger, and R. F. Sekerka, "Convective and Interfacial Stabilities During Unidirectional Solidification," *J. Crystal Growth*, **49**, 13 (1980).

Coriell, S. R., R. F. Boisvert, R. G. Rehm, and R. F. Sekerka, "Lateral Solute Segregation During Unidirectional Solidification and Interface Instabilities During Unidirectional Solidification of a Binary Alloy," *J. Crystal Growth*, **54**, 167 (1981).

Cormack, D. E., L. G. Leal, and J. Imberger, "Natural Convection in a Shallow Cavity with Differentially Heated End Walls. 1: Asymptotic Theory," *J. Fluid Mech*, **65**, 209 (1974).

Crochet, M. J., P. J. Wouters, F. T. Geyling, and A. S. Jordan, "Finite-Element Simulation of Czochralski Bulk Flow," *J. Crystal Growth*, **65**, 153 (1983).

Crochet, M. J., F. T. Geyling, and J. J. Van Schaftinger, "Numerical Simulation of the Horizontal Bridgman Process. I: Two-dimensional Flow," *Int. J. Num. Meth. Fluids*, **7**, 29 (1987).

———"Numerical Simulation of Horizontal Bridgman Growth. II: Three-dimensional Flow," *Int. J. Numer. Meth. Fluids*, **7**, 49 (1987b).

Crowley, A. B., "Mathematical Modeling of Heat Flow in Czochralski Crystal Pulling" *IMA J. Appl. Math.*, **30**, 173 (1983).

Curry, J. H., J. R. Jackson, J. Loncaris, and S. A. Orszag, "Order and Disorder in Two- and Three-dimensional Benard Convection," *J. Fluid Mech.*, **147**, 1 (1984).

Davis, S. H., U. Muller, and C. Dietsche, "Pattern Selection in Single-Component Systems Coupling Benard Convection and Solidification," *J. Fluid Mech.*, **144**, 133 (1984).

Davis, S. H., "Thermocapillary Instabilities," *Ann. Rev. Fluid Mech.*, **19**, 403 (1987).

Derby, J. J., and R. A. Brown, "A Fully Implicit Method for Simulation of the One-Dimensional Solidification of a Nondilute Binary Alloy," *Chem. Eng. Sci.*, **41**, 37 (1986a).

———, "Thermal-Capillary Analysis of Czochralski and Liquid-Encapsulated Czochralski Crystal Growth. I: Steady State Simulation," *J. Crystal Growth*, **74**, 605 (1986b).

———, "Thermal-Capillary Analysis of Czochralski and Liquid-Encapsulated Czochralski Crystal Growth. II: Processing Strategies," *J. Crystal Growth*, **75**, 227 (1986c).

———, "The Dynamics of Czochralski Crystal Growth," *J. Crystal Growth*, **83**, 137 (1987).

———, "On the Quasisteady-state Assumption in Modeling Batchwise Czochralski Growth," *J. Crystal Growth*, **87**, 251 (1988).

Derby, J. J., R. A. Brown, F. T. Geyling, A. S. Jordan, and G. A. Nikolakopoulou, "A Thermal-Capillary Model for Liquid-Encapsulated Czochralski Growth," *J. Electrochem. Soc.*, **132**, 470 (1985).

Derby, J. J., L. J. Atherton, P. D. Thomas, and R. A. Brown, "Finite-Element Methods for Analysis of the Dynamics and Control of Czochralski Crystal Growth," *J. Sci. Computing*, **2**, 297 (1988).

Dietl, J., D. Helmreich, and E. Sirtl, "Solar Silicon," *Crystals: Growth, Properties and Applications*, **5**, J. Grabmaier, ed., Springer, Berlin, 43 (1981).

Dillion, O. W., C. T. Tsai, and R. J. Angelis, "Dislocation Dynamics During the Growth of Silicon Ribbon," *J. Crystal Growth*, **82**, 50 (1987).

Duseaux, M., "Temperature Profile and Thermal Stress Calculations in GaAs Crystals Growing from the Melt, " *J. Crystal Growth*, **61**, 576 (1983).

Dupret, F., Y. Ryckmans, P. Wouters, and M. J. Crochet, "Numerical Calculation of Global Heat Transfer in a Czochralski Furnace," in *Crystal Growth 1986*, B. Cockayne, J. H. C. Hogg, B. Lunn, P. J. Wright, eds.; North-Holland, New York, 84 (1986).

Duranceau, J. L., and R. A. Brown, "A Thermal-Capillary Model for the Floating Zone Crystal Growth Process," *J. Crystal Growth*, **75**, 367 (1986).

Flemings, M. C., *Solidification Processing*, McGraw-Hill, New York, (1974).

Fornari, R., C. Paorici, L. Zanotti, and G. Zuccalli, "Dislocation-free Silicon-doped Gallium Arsenide Grown by LEC Procedure," *J. Crystal Growth*, **63**, 415 (1983).

Gault, W. A., E. M. Monberg, and J. E. Clemens, "A Novel Application of the Vertical Gradient Freeze Method to the Growth of High-quality III-V Crystals," *J. Crystal Growth*, **74**, 491 (1986).

Glicksman, M. E., S. R. Coriell, and G. B. McFadden, "Interaction of Flows with the Crystal-Melt Interface," *Ann. Rev. Fluid Mech.*, **18**, 307 (1986).

Guckenheimer, J., and P. Holmes, *Nonlinear Oscillations, Dynamical Systems, and Bifurcations of Vector Fields;* Springer, New York, (1983).

Guruswamy, S., R. S. Rai, K. T. Faber, and J. P. Hirth, "Deformation Behavior of Undoped and In-doped GaAs in the Temperature Range 700°C to 1,000°C," *J. Appl. Phys.*, **62**, 4130 (1987).

Haasen, P., "Dislocation Dynamics in the Diamond Structure," in *Dislocation Dynamics*, A. R. Rosenfield, G. T. Hahn, A. L. Bement, I Jaffee, eds., Battelle Inst. Materials Colloq. (1967).

Hardy, S., "The Surface Tension of Liquid Silicon," *J. Crystal Growth*, **69**, 456 (1984).

Harriott, G. M., and R. A., Brown, "Flow Structure and Radial Dopant Segregation in Small-Scale Floating Zones," *J. Crystal Growth*, **69**, 589 (1984).

Hart, J. E., "Low Prandtl Number Convection Between Differentially Heated Walls," *Int. J. Heat Mass Trans.* **26**, 1069 (1983a).

———, "A Note on the Stability of Low Prandtl Number Hadley Circulations," *J. Fluid Mech.*, **132**, 271 (1983b).

Haynes, J. M., "Capillarity and Wetting," *Materials Sciences in Space*, B. Feuerbacher, H. Hamacher, R. J. Naumann, eds., Springer, Berlin, 129 (1986).

Herring, C., in *The Physics of Powder Metallurgy*, W. E. Kingston, ed., McGraw-Hill, New York (1951).

Hjellming, L. N., and J. S. Walker, "Melt Motion in a Czochralski Crystal Puller with an Axial Magnetic Field: Isothermal Motion," *J. Fluid Mech.*, **164**, 237 (1986).

———, "Melt Motion in a Czochralski Crystal Puller with an Axial Magnetic Field: Uncertainty in the Thermal Constants," *J. Crystal Growth*, **87**, 18 (1988).

———, "Mass Transport in a Czochralski Puller with a Strong Magnetic Field," *J. Crystal Growth*, **85**, 25 (1987).

Homsy, G. M., and E. Meiburg, "The Effect of Surface Contamination on Thermocapillary Flow in a Two-dimensional Slot," *J. Fluid Mech.*, **139**, 443 (1984).

Hoshikawa, I., H. Kohda, H. Nakanishi, and K. Ikuta, "Low Oxygen Content Czochralski Silicon Crystal Growth," *Japan J. Appl. Phys.*, **19**, 133 (1980).

Huh, C., and L. E. Scriven, "Shapes of Axisymmetric Fluid Interfaces of Unbounded Extent," *J. Colloid. Interf. Sci.*, **30**, 323 (1969).

Hurle, D. T. J., "Control of Diameter in Czochralski and Related Crystal Growth Techniques," *J. Crystal Growth*, **42**, 473 (1977).

———, "Analytical Representation of the Shape of the Meniscus in Czochralski Growth," *J. Crystal Growth*, **63**, 13 (1983).

———, "Stability of Melt Growth Processes," *Crystal Growth of Electronic Materials*, E. Kaldis ed., Elsevier, New York, (1985).

Hurle, D. T. J., and R. W. Series, "Effective Distribution Coefficient in Magnetic Czochralski Growth," *J. Crystal Growth*, **73**, 1 (1985).

Hurle, D. T. J., E. Jakeman, and E. R. Pike, "Striated Solute Distribu-

tions Produced by Temperature Oscillations During Crystal Growth from the Melt," *J. Crystal Growth*, **34**, 633 (1968).
Hurle, D. T. J., E. Jakeman, and C. P. Johnson, "Convection Temperature Oscillations in Molten Gallium," *J. Fluid Mech.*, **64**, 565 (1974).
Hurle, D. T. J., G. C. Joyce, G. C. Wilson, M. Ghassempoory, and C. Morgan, "A Technique for Experimentally Determining the Transfer Function of a Czochralski Pulling Process," *J. Crystal Growth*, **74**, 480 (1986).
Jacob, G., "How to Decrease Defect Densities in LEC Si, GaAs, and InP Crystals," *Proc. Semi-Insulating III-V Materials Conf.*, Evian, 2 (1982).
Jasinski, T. J., and A. F. Witt, "On Control of the Interface Shape During Growth in Vertical Bridgman Configuration," *J. Crystal Growth*, **71**, 295 (1985).
Jasinski, T. J., W. M. Rohsensow, and A. F. Witt, "Heat Transfer Analysis of the Bridgman-Stockbarger Configuration for Crystal Growth. I: Analytical Treatment of the Axial Temperature Profile," *J. Crystal Growth*, **61**, 339 (1983).
Jordan, A. S., A. R. Caruso, and A. R. Von Neida, "A Thermoelastic Analysis of Dislocation Generation in Pulled GaAs Crystals," *Bell System Tech. J.*, **59**, 593 (1980).
Jordon, A. S., A. R. Caruso, A. R. Von Neida, and J. W. Nielsen, "A Comparative Study of Thermal Stress Induced Dislocation Generation in Pulled GaAs, InP, and Si Crystals," *J. Appl. Physics*, **52**, 3331 (1981).
Jordan, A. S., "Estimated Thermal Diffusivity, Prandtl Number and Grashof Number of Molten GaAs, InP and GaSb," *J. Crystal Growth*, **71**, 551 (1985).
Karma, A., "Solidification Cells at Low Velocity: The Moving Symmetric Model," *Phys. Rev. A.*, **34**, 4353 (1986).
Kakimoto, K., and T. Hibiya, "Temperature Dependence of Viscosity of Molten GaAs by an Oscillation Cup Method," *Appl. Phys. Lett.*, **50**, 12 (1987).
Kim, D.-H, Ph.D. Thesis, Mass. Inst. Technol., in preparation.
Kim, D.-H., P. M. Adornato, and R. A. Brown, "Effect of Vertical Magnetic Field on Convection and Segregation in Vertical Bridgman Crystal Growth," *J. Crystal Growth*, in press (1988).
Kim, K. M., "Suppression of Thermal Convection by Transverse Magnetic Field," *J. Electrochem. Soc.*, **132**, 427 (1982).
Kim, K. M., and W. E. Langlois, "Computer Simulation of Boron Transport in Magnetic Czochralski Growth of Silicon," *J. Electrochem. Soc.*, **133**, 2590 (1986).
Kim, K. M., and P. Smetana, "Oxygen Segregation in CZ Silicon Crystal Growth on Applying a High Axial Magnetic Field," *J. Electrochem. Soc.*, **133**, 1682 (1986).
Kim, K. M., A. F. Witt, and H. Gatos, "Crystal Growth from the Melt Under Destabilizing Thermal Gradients," *J. Electrochem. Soc.*, **119**, 1218 (1972).
Kim, K. M., A. F. Witt, M. Lichtensteiger, and H. C. Gatos, "Quantitative Analysis of the Effects of Destabilizing Vertical Gradients on Crystal Growth and Segregation: Ga-doped Ge," *J. Electrochem. Soc.*, **125**, 475 (1978).
Kim, K. M., A. Kran, P. Smetana, and G. H. Schwuttke, "Computer Simulation and Controlled Growth of Large-Diameter Czochralski Silicon Crystals," *J. Electrochem. Soc.*, **130**, 1156 (1983).
Kobayashi, N., "Computational Simulation of the Melt Flow During Czochralski Growth," *J. Crystal Growth*, **43**, 357 (1978).
———, "Heat Transfer in Czochralski Crystal Growth," *Preparation and Properties of Solid State Materials*, **6**, W. R. Wilcox ed., Dekker, New York (1981).
Kobayashi, N., and T. Iwaki, "A Thermoelastic Analysis of the Thermal Stress Produced in a Semiinfinite Cylindrical Single Crystal During the Czochralski Growth," *J. Crystal Growth*, **73**, 96 (1985).
Kuroda, E., and H. Kozuka, "Influence of Growth Conditions on Melt Interface Temperature Oscillations in Silicon Czochralski Growth," *J. Crystal Growth*, **63**, 276 (1983).
Lambropoulos, J. C., "Stresses Near the Solid-Liquid Interface During the Growth of a Czochralski Crystal," *J. Crystal Growth*, **80**, 245 (1987).
Lambropoulos, J. C., J. W. Hutchinson, R. O. Bell, B. Chalmers, and J. P. Kalejs, "Plastic Deformation Influence on Stress Generation During Silicon Sheet Growth at High Speeds," *J. Crystal Growth*, **65**, 324 (1983).
Langer, J. S., and D. C. Hong, "Solvability Conditions for Dendritic Growth in a Boundary-Layer Model with Capillary Anisotropy," *Phys. Rev. A.*, **34**, 1462 (1986).
Langlois, W. E., "A Parameter Sensitivity Study for Czochralski Bulk Flow of Silicon," *J. Crystal Growth*, **56**, 15 (1982).
———, "Computer Simulation of Czochralski Melt Convection in a Magnetic Field," *J. Crystal Growth*, **70**, 73 (1984).
———, "Buoyancy-Driven Flows in Crystal Growth Melts," *Ann. Rev. Fluid Mech.*, **17**, 191 (1985).
Langlois, W. E., and J. S. Walker, "Czochralski Crystal Growth in an Axial Magnetic Field," *Computational and Asymptotic Methods for Boundary and Interior Layers, Proc. BAIL II Conf.* (1982).
Lee, K. J., W. E. Langlois, and K. M. Kim, "Digital Simulation of Oxygen Transfer and Oxygen Segregation in Magnetic Czochralski Growth of Silicon," *Physicochem. Hydrodyn.*, **5**, 135 (1984).
Levich, V. G., *Physicochemical Hydrodynamics*, Prentice-Hall, Englewood Cliffs, NJ (1962).
Lin, W., and Benson, K. E., "The Science and Engineering of Large-Diameter Czochralski Silicon Crystal Growth, " *Ann. Rev. Mater. Sci.*, **17**, 293 (1987).
McGuigan, S., R. N. Thomas, D. L. Barnett, H. M. Hobgood, and B. W. Swanson, *Appl. Phys. Lett.*, **48**, 1377 (1986).
McLaughlin, J., and S. A. Orszag, "Transition from Periodic to Chaotic Thermal Convection," *J. Fluid Mech.*, **123**, 123 (1982).
Mihelcic, M., and K. Winegrath, "Numerical Simulations of the Czochralski Bulk Flow in an Axial Magnetic Field: Effects on the Flow and Temperature Oscillations in the Melt," *J. Crystal Growth*, **71**, 163 (1985).
Mihelcic, M., K. Winegrath, and Chr. Pirron, "Three-dimensional Simulations of the Czochralski Bulk Flow," *J. Crystal Growth*, **69**, 473 (1984).
Mika, K., and W. Uelhoff, "Shape and Stability of Meniscus in Czochralski Growth and Comparison with Analytical Approximations," *J. Crystal Growth*, **30**, 9 (1975).
Mil'vidskii, M. G., V. B. Osvenskii, and S. S. Shifrin, "Effect of Doping on Formation of Dislocation Structure in Semiconductor Materials," *J. Crystal Growth*, **52**, 396 (1981).
Muhlbauer, A., and W. Keller, *Floating Zone Silicon*, Dekker, New York (1981).
Muhlbauer, A., W. Erdmann, and W. Keller, "Electrodynamic Convection in Silicon Floating Zones," *J. Crystal Growth*, **64**, 529 (1983).
Mullins, W. W., and R. F. Sekerka, "Morphological Stability of a Particle Growing by Diffusion of Heat Flow," *J. Appl. Phys.*, **34**, 323 (1963).
———, "Stability of a Planar Interface During Solidification of a Dilute Binary Alloy," *J. Appl. Phys.*, **35**, 444 (1964).
Murgai, A., "Oxygen Incorporation in Czochralski Silicon," *Crystal Growth of Electronic Materials*, E. Kaldis ed., Elsevier, New York, 211 (1985).
Myshlyaev, M., V. I. Nikitenko, and V. I. Nestenenko, "Dislocation Structure and Macroscopic Characteristics of Plastic Deformation at Creep of Silicon Crystals," *Phys. Stat. Sol.*, **36**, 89 (1969).
Naumann, R. J., "An Analytical Approach to Thermal Modeling of Bridgman-type Crystal Growth. 1: One-dimensional Analysis," *J. Crystal Growth*, **58**, 589 (1983).
Naumann, R. J., and S. L. Lehoczky, "Effect of Variable Thermal Conductivity on Isotherms in Bridgman Growth," *J. Crystal Growth*, **61**, 707 (1983).
Nernst, W., "Theorie der Reaktionsgeschwindigkeit in heterogenen Systemen," *Z. Phys. Chem.*, **47**, 52 (1904).
Ono, H., H. Watanabe, T. Kamejima and J. Matsui, "Cellular Growth and In Concentrated Inclusions in LEC In-doped GaAs Crystals," *J. Crystal Growth* **74**, 446 (1986).
Oreper, G. M., and J. Szekely, "The Effect of an Externally Imposed Magnetic Field on Buoyancy-Driven Flow in a Rectangular Cavity," *J. Crystal Growth*, **64**, 505 (1983).
———, "The Effect of a Magnetic Field on Transport Phenomena in a Bridgman-Stockbarger Crystal Growth," *J. Crystal Growth*, **67**, 405 (1984).
Padday, J. F., "The Profiles of Axially Symmetric Menisci," *Philos. Trans. Royal Soc. Lond.*, **269**, 23 (1971).
Pan, Y. F., and A. Acrivos, "Heat Transfer at High Peclet Number in Regions of Closed Streamlines," *Int. J. Heat Mass Trans.*, **11**, 439 (1968).

Parsey, J. M., and G. A. Thiel, "A New Apparatus for the Controlled Growth of Single-Crystals by Horizontal Bridgman Techniques," *J. Crystal Growth,* **73,** 211 (1985).
Pearson, J. R. A., "On Convection Cells Induced by Surface Tension," *J. Fluid Mech.,* **4,** 2125 (1958).
Pfann, W. G., *Zone Melting,* Krueger, Huntington, NY (1978).
Pimputkar, S. M., and S. Ostrach, "Convective Effects in Crystal Growth from Melt," *J. Crystal Growth,* **55,** 614 (1981).
Preisser, G., D. Schwabe, and A. Scharmann, "Steady and Oscillatory Thermocapillary Convection in Liquid Columns with Free Cylindrical Surfaces," *J. Fluid Mech.,* **126,** 545 (1982).
Ramachandran, P. A., and M. P. Dudokovic, "Simulation of Temperature Distributions in Crystals Grown by Czochralski Method," *J. Crystal Growth,* **71,** 399 (1985).
Ravi, K. V., *Imperfections and Impurities in Semiconductor Silicon,* Wiley, New York (1981).
Robertson, D. S., and I. M. Young, "Observations on the Unrestrained Growth of Germanium Crystals," *J. Phys. D: Appl. Phys.,* **8,** L59 (1975).
Robertson, G. D., Jr., and D. J. O'Connor, "Magnetic Field Effects on Float-Zone Si Crystal Growth. I: Strong Transverse Fields," *J. Crystal Growth,* **76,** 111 (1986).
Rosenberger, F., *Fundamentals of Crystal Growth,* Springer, New York (1979).
Rouzaud, A., D. Camel, and J. J. Favier, "A Comparative Study of Thermal and Thermosolutal Convective Effects in Vertical Bridgman Crystal Growth," *J. Crystal Growth,* **73,** 149 (1985).
Rowlinson, J. S., and B. Widom, *Molecular Theory of Capillarity,* Clarendon Oxford (1982).
Sackinger, P., R. A. Brown, and G. B. McFadden, "Eigenfunction Expansions for Determining-Structure of Natural Convection in a Vertical Cylinder Heated from Below," *J. Fluid Mech.,* submitted (1988a).
Sackinger, P. A., J. J. Derby, and R. A. Brown, "Axisymmetric Convection in a Complete Thermal-Capillary for Czochralski Crystal Growth," *Int. J. Num. Meths. Fluids,* (1988b).
Scheil, E., "Bemerkungen zur Schichtkristallbildung," *Z. Metallk,* **34,** 70 (1942).
Schroter, W., H. G. Brion, and H. Siethoff, "Yield Point and Dislocation Mobility in Silicon and Germanium," *J. Appl. Phys.,* **54,** 1816 (1983).
Scriven, L. E., and C. V. Sternling, "On Cellular Convection Driven by Surface-Tension Gradients: Effects of Mean Surface Tension and Surface Viscosity," *J. Fluid Mech.,* **19,** 321 (1964).
Sen, A. K., and S. H. Davis, "Steady Thermocapillary Flows in Two-dimensional Slots," *J. Fluid Mech.,* **121,** 163 (1982).
Series, R. W., D. T. J. Hurle, and K. G. Barraclough, "Effective distribution Coefficient of Silicon Dopants During Magnetic Czochralski Growth," *IMA J. Appl. Math.,* **35** (1985).
Singh, R., A. F. Witt, and H. C. Gatos, "Application of the Peltier Effect for the Determination of Crystal Growth Rates," *J. Electrochem. Soc.,* **115,** 747 (1968).
Smith, M. C., and Davis, S. H., "The Instability of Sheared Liquid Layers," *J. Fluid Mech.,* **121,** 187 (1982).
———, "Instabilities of Dynamic Thermocapillary Liquid Layers. 1: Convective Instabilities," *J. Fluid Mech.,* **132,** 119 (1983a).
———, "Instabilities of Dynamic Thermocapillary Liquid Layers. 2: Surface-wave Instabilities," *J. Fluid Mech.,* **132,** 145 (1983b).
Smith, V. G., W. A. Tiller, and B. Chalmers, "A Mathematical Analysis of Solute Redistribution During Solidification," *Can. J. Physics,* **33,** 723 (1955).
Sneyd, A. D., "Fluid Flow Induced by a Rapidly Alternating or Rotating Field," *J. Fluid Mech.,* **92,** 35 (1979).
Sristava, R. K., P. A. Ramachandran, and M. P. Dudokovic, "Interface Shape in Czochralski Grown Crystals: Effects of Conduction and Radiation," *J. Crystal Growth,* **73,** 487 (1985).
Steel, G. K., and M. J. Hill, "Analysis of the Heat Transfer Function Governing Crystal Growth in the Czochralski Process," *J. Crystal Growth,* **30,** 45 (1975).
Stephanopoulos, G., *Chemical Process Control,* Prentice-Hall, Englewood Cliffs, NJ (1984).
Suezawa, M., K. Sumino, and I. Yonenaga, "Dislocation Dynamics in the Plastic Deformation of Silicon Crystals," *Phys. Stat. Sol.,* **51,** 217 (1979).
Sumino, K., H. Harada, and I. Yonenaga, "The Origin of the Difference in the Mechanical Strengths of Czochralski-grown Silicon and Float Zone Grown Silicon," *Japan J. Appl. Phys.,* **19,** L49 (1980).
Surek, T., "Theory of Shape Stability in Crystal Growth from the Melt," *J. Appl. Phys.,* **47,** 4384 (1976).
Surek T., and B. Chalmers, "The Direction of Growth of the Surface of a Crystal in Contact with its Melt," *J. Crystal Growth,* **29,** 1 (1975).
Surek, T., S. R. Coriell, and B. Chalmers, "The Growth of Shaped Crystals from the Melt," *J. Crystal Growth,* **50,** 21 (1980).
Tabache, M. G., E. D. Bouret, and A. G. Elliot, "Effect of the Critical Resolved Shear Stress for Indium-Doped and -Undoped GaAs Single Crystals," *Appl. Phys. Lett.,* **49,** 289 (1986).
Tangborn, "Numerical simulation of Czochralski bulk flow," Ph.D. Thesis, Mass. Inst. Technol. (1987).
Tatarchenko, V. A., and E. A. Brener, "Crystallization Stability During Capillary Shaping. I: General Theory of Capillary and Thermal Stability," *J. Crystal Growth,* **50,** 33 (1980).
Thomas, P. J., R. A. Brown, J. J. Derby, L. J. Atherton, and M. J. Wargo, "Simulation and Control of Seeding in Liquid-Encapsulated Czochralski Growth of GaAs: Comparison Between Simulation and Experiment," *J. Crystal Growth,* submitted (1988).
Tiller, W. A., K. A. Jackson, J. W. Rutter, and B. Chalmers, "The Redistribution of Solute Atoms During the Solidification of Metals," *Acta Met.,* **1,** 428 (1953).
Trivedi, R., and K. Somboonsuk, "The Effect of Growth Rate on Interface Morphology," *Proc. Flat-Plate Solar Array Research Forum on High-Speed Growth and Characterization of Crystals for Solar Cells,* Jet Propul. Lab. Pub. No. 84-23 (1984).
Tsavinsky, S. V., "Dislocation Density in Pure Crystals Grown from Melts," *Kristall. Tech.,* **10,** 5 (1979).
Turner, J. S., *Buoyancy Effects in Fluids,* Cambridge Univ. Press, (1973).
Ungar, L. H., and R. A. Brown, "Cellular Interace Morphologies in Directional Solidification. 1: The One-sided Model," *Phys. Rev. B,* **29,** 1367 (1984).
———, "Cellular Interface Morphologies in Directional Solidification. 4: The Formation of Deep Cells," *Phys. Rev. B,* **31,** 5831 (1985).
Ungar, L. H., M. J. Bennett, and R. A. Brown, "Cellular Interface Morphologies in Directional Solidification. 3: The Effect of Coupled Heat Transfer," *Phys. Rev. B,* **31,** 5923 (1985).
Utech, H., and M. C. Flemings, "Elimination of Solute Banding in Indium Antimonide Crystals by Growth in a Magnetic Field," *J. Appl. Phys.,* **37,** 2021 (1966).
Wang, C. A., Ph.D. Thesis, "Crystal Growth and Segregation in Vertical Bridgman Configuration," Mass. Inst. Technol. (1984).
Wang, C. A., A. F. Witt, and J. R. Carruthers, "Thermal Characteristics of a Heat-Pipe Based Vertical Bridgman Growth System," *J. Crystal Growth,* **66,** 299 (1984).
Wargo, M. J., and A. F. Witt, "Determination of the Peltier Coefficient from Current-Induced Growth Layers: InSb/Melt," *J. Crystal Growth,* **66,** 289 (1984).
Wilcox, W. R., "Validity of the Stagnant-Film Approximation for Mass Transfer in Crystal Growth and Dissolution," *Mat. Res. Bull,* **4,** 265 (1969).
Williams, G., and W. E. Reusser, "Heat Transfer in Silicon Czochralski Crystal Growth," *J. Crystal Growth,* **64,** 448 (1983).
Wilson, L. O., "On Interpreting a Quantity in the Burton, Prim, and Slichter Equation as a Diffusion Boundary Layer Thickness," *J. Crystal Growth,* **44,** 247 (1978a).
———, "A New Look at the Burton, Prim, and Slichter Model of Segregation During Crystal Growth from the Melt," *J. Crystal Growth,* **44,** 371 (1978b).
———, "The Effect of Fluctuating Growth Rates on Segregation in Crystals Grown from the Melt. I: No Backmelting," *J. Crystal Growth,* **48,** 435 (1980a).
———, "The Effect of Fluctuating Growth Rates on Segregation in Crystals Grown from the Melt. II: Backmelting," *J. Crystal Growth,* **48,** 451 (1980b).
Winters, K. H., "Oscillatory Convection in Crystal Melts: The Horizontal Bridgman Process," *Proc. 5th Int. Conf. Num. Meth. in Thermal Problems,* Pineridge Press (1987).
Witt, A. F., N. Lichtensteiger, and H. C. Gatos, "Experimental Approach to the Quantitative Determination of Dopant Segregation

During Crystal Growth on a Microscale," *J. Electrochem. Soc.*, **120**, 1119 (1983).
Woodruff, D. P., *The Solid-Liquid Interface;* Cambridge Press, Cambridge (1973).
Wouters, P., J. J. Van Schaftingen, M. J. Crochet, and F. T. Geyling, "Numerical Simulation of the Horizontal Bridgman Growth. III: Calculation of the Interface," *Int. J. Num. Meth. Fluids*, **7**, 131 (1987).
Zief, M., and W. R. Wilcox, *Fractional Solidification*, Dekker, New York (1967).
Zulehner, W., and D. Huber, "Czochralski-Grown Silicon," *Crystals: Growth, Properties and Applications*, **8** J. Grabmaier, ed., Springer, New York, 1 (1982).

Manuscript received Sept. 16, 1987, and revision received Feb. 29, 1988.

Robert A. Brown is a native of San Antonio, Texas, and did his initial studies in chemical engineering at the University of Texas at Austin where he received a B.S. in 1973 and M.S. in 1975. He received a Ph.D. in 1979 from the University of Minnesota after completing his thesis on the shape and stability of drops and bubbles with L.E. Scriven. His thesis work included a stay at Lawrence Berkeley Laboratories. He joined the faculty at M.I.T. in 1979 and presently holds the Arthur D. Little Professorship there. His research program focuses on modelling transport processes in material processing systems, especially solidification phenomena and non-Newtonian fluid mechanics, and on the development of numerical methods for analysis of these systems. When he is not tending to this research program or teaching, he focuses his energy at keeping up with his two small boys and their vigorous mother.